CHALMERS

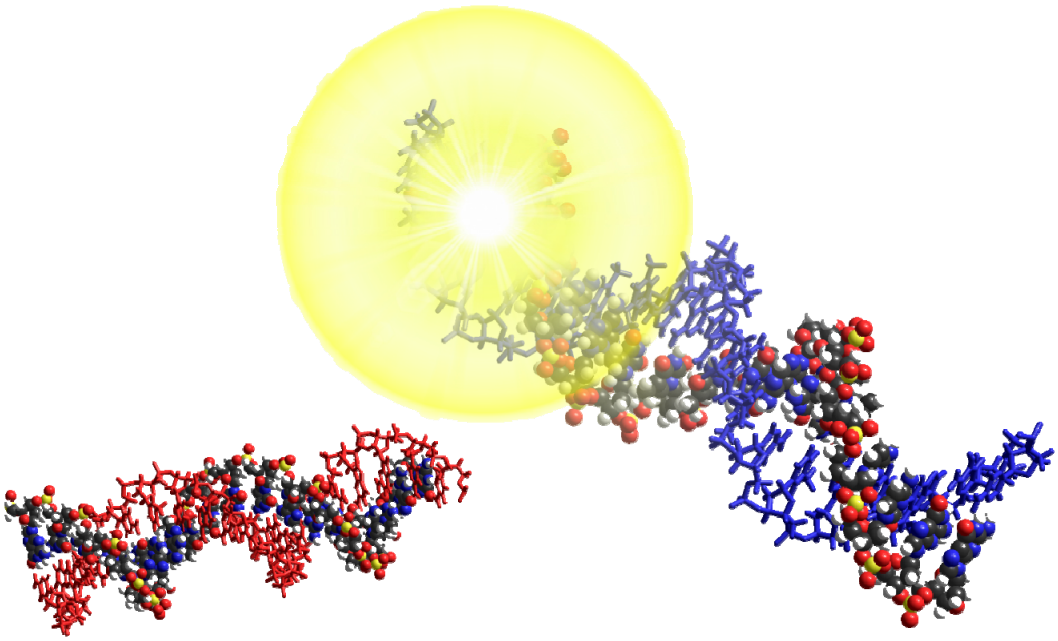

In Vitro Catalysis of DNA Strand Exchange:

Novel Insights into the Activity of Nucleic Acids on a Molecular Level

Master of Science Thesis

BOBO FENG

Department of Chemical and Biological Engineering
Division of Physical Chemistry
CHALMERS UNIVERSITY OF TECHNOLOGY
Gothenburg, Sweden, 2010

THESIS FOR THE DEGREE OF MASTER OF SCIENCE

In Vitro Catalysis of DNA Strand Exchange:

Novel Insights into the Activity of Nucleic Acids on a Molecular Level

Bobo Feng

CHALMERS

Department of Chemical and Biological Engineering
CHALMERS UNIVERSITY OF TECHNOLOGY
Gothenburg, Sweden, 2010

In Vitro Catalysis of DNA Strand Exchange:
Novel Insights into the Activity of Nucleic Acids on a Molecular Level

Bobo Feng

Department of Chemical and Biological Engineering
Chalmers University of Technology
SE-412 96 Göteborg
Sweden
Telephone + 46 (0)31-772 1000

Cover picture:
DNA activity in new light. Recovery of FAM emission from fluorescently labeled DNA duplexes due to decreased FRET quenching allows direct monitoring of DNA strand exchange kinetics (explained in Figure 6.2).

Department of Chemical and Biological Engineering
Göteborg, Sweden 2010

In Vitro Catalysis of DNA Strand Exchange:
Novel Insights into the Activity of Nucleic Acids on a Molecular Level

Bobo Feng

Department of Chemical and Biological Engineering
Chalmers University of Technology

ABSTRACT

Strand exchange between single and double stranded DNA is the basis for DNA repair and maintenance of genetic diversity *in vivo*, but the biocatalytic mechanism of recombination proteins like RecA and Rad51 is not known in detail. To better understand the role of environment at the active sites of recombinases, this thesis studies artificial strand exchange catalysis, and the behavior of DNA, in biomimetic model systems using melting curves, FRET, and CD spectroscopy.

Polyarginine was found to accelerate strand exchange while stabilizing the double helix, with a high concentration of arginine residues along the polypeptide vital for its activity. Furthermore, a peptide:dsDNA charge ratio of 1 proved optimal, while yields significantly decreased for higher peptide concentrations. This is linked to evidence for the formation of highly compacted and inert polyarginine-DNA complexes.

The crowded environment within recombinase-DNA filaments was recreated using macromolecular polymers in a fundamentally new approach. The rate of strand exchange is accelerated by several orders of magnitude in the presence of PEG-6000 and increases rapidly with PEG concentration. Strand exchange in PEG solutions proceeds under conditions which preserve the overall duplex stability and B-DNA conformation, with the key step being helix breathing promoted by the nonpolar environment. The results presented in this thesis highlight the importance of hydrophobic interactions between DNA and proteins, and may have a lasting impact on how the relationship between DNA stability and activity is perceived.

Keywords: DNA, strand exchange, synthetic biology, catalysis, FRET spectroscopy, polyarginine, polyethylene glycol, molecular crowding, base stacking.

List of abbreviations

A	Adenine, a DNA base, or absorbance (in Chapter 5.2)
B-DNA	Prevalent DNA conformation *in vivo*
C	Cytosine, a DNA base
CD	Circular dichroism
DME	Dimethoxyethane
DNA	Deoxyribonucleic acid
DOPC	1,2-Dioleoyl-sn-glycero-3-phosphatidylcholine, a lipid
DOPG	1,2-Dioleoyl-sn-glycero-3-phospho-rac-(1-glycerol) sodium salt, a lipid
DOTAP	N-[1-(2,3-dioleoyloxy)propyl]-N,N,N-trimethylammonium chloride, a lipid
dsDNA	Double stranded DNA
DSPE-MPEG	1,2-distearoyl-sn-glycero-3-phosphoethanolamine-N-[poly(ethylene glycol) 2000], a lipid
FAM	Carboxyfluorescein, a fluorescent dye
FRET	Förster resonance energy transfer (fluorescence resonance energy transfer)
G	Guanine, a DNA base
HPLC	High pressure liquid chromatography (High performance liquid chromatography)
K	Lysine, an amino acid
k	Rate constant
m_x	Mismatched oligonucleotide, single strand
O_x	Oligonucleotide, single strand
PBS	Phosphate buffered saline
PEG	Polyethylene glycol
Psi-DNA	DNA conformation induced by polymers and salt
R	Arginine, an amino acid
r^2	Coefficient of determination
Rad51	Recombinase encoded by human RAD51 gene and eukaryotic homologs
RecA	Recombinase, prokaryotic homolog to Rad51
RNA	Ribonucleic acid
ssDNA	Single stranded DNA
T	Thymine, a DNA base
T_m	Melting temperature for DNA
TAMRA	Tetramethylrhodamine, a fluorescent dye
W	Tryptophan, an amino acid
ε	Dielectric constant
τ	Inverted rate constant

Table of contents

1 Introduction

Deoxyribonucleic acid (DNA) is the universal carrier of genetic information and the template for protein synthesis.[1] The basis for DNA repair and maintenance of genetic diversity is homologous recombination, exchange of strands between double and single stranded DNA with identical or similar sequence. This kinetically disfavored process is catalyzed enzymatically by recombinases like RecA in prokaryotes and Rad51 in eukaryotes.[2-4]

Structures of RecA[5] and Rad51[6] filaments in complex with DNA have recently been presented, but research into their biomolecular function *in vivo* is difficult due to the complexity of biological systems. Despite intense structural and functional investigations, the active form of the protein-DNA complex and the mechanism of strand exchange biocatalysis are not understood in detail.[7-10]

In addition to recombinases, other agents like liposomes[11], polypeptides[12], and synthetic polymers[13] have been reported to catalyze strand exchange *in vitro*. Being important proofs of concept, the proposed mechanisms of these catalysts involve high concentrations of positive charges clearly different from the hydrophobic conditions found in proteins.

The aim of this project is to deduce how recombinases work, especially which conditions are present at their active sites, through invention and use of biomimetic model systems for strand exchange catalysis. The advantage of model systems, apart from their relative simplicity, is sufficient robustness to allow systematic variation of environmental factors governing DNA activity such as temperature, hydrophobicity, and ionic strength.

Firstly, the catalytic activities of hydrophobic and lightly charged polypeptides have been investigated. Design of peptide sequences was aided by examination of bacterial RecA protein structure and simple molecular modeling of peptide-DNA interactions. Peptides at different concentrations both in solution and immobilized on beads and liposomes were used, and the strand exchange reaction kinetics was monitored with FRET between labeled synthetic DNA oligonucleotides.

Secondly, method developments of FRET in viscous media enabled studies of the two biocompatible polymers dextran and polyethylene glycol (PEG), where DNA is subjected to crowded conditions and low water activity. Special attention was given to critical effects in the more hydrophobic PEG-water system, including kinetic tracing at ambient and physiological temperature, at different PEG and salt concentrations, and with DNA mismatched at various positions.

2 DNA

According to the central dogma of microbiology outlined in Figure 2.1, genetic information stored by DNA ultimately defines the structure of proteins, building blocks of living matter. Without DNA repair through homologous recombination, deleterious mutational defects will accumulate over time.

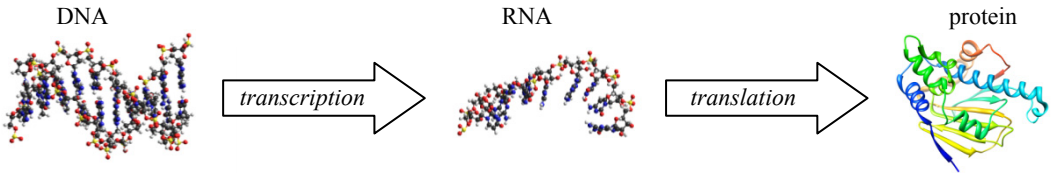

Figure 2.1. The central dogma of microbiology illustrates the flow of information from DNA to protein sequence.

DNA is naturally found both in single and double stranded forms. Single stranded DNA (ssDNA) is a linear polymer of individual nucleotides, each consisting of a DNA base, a deoxyribose sugar, and a phosphate group carrying a single negative net charge (see Figure 2.2). The base sequence constitutes the genetic code and is read from the 3' to the 5' end. Double stranded DNA (dsDNA) consists of two noncovalently joined single strands with the second strand in opposite direction.

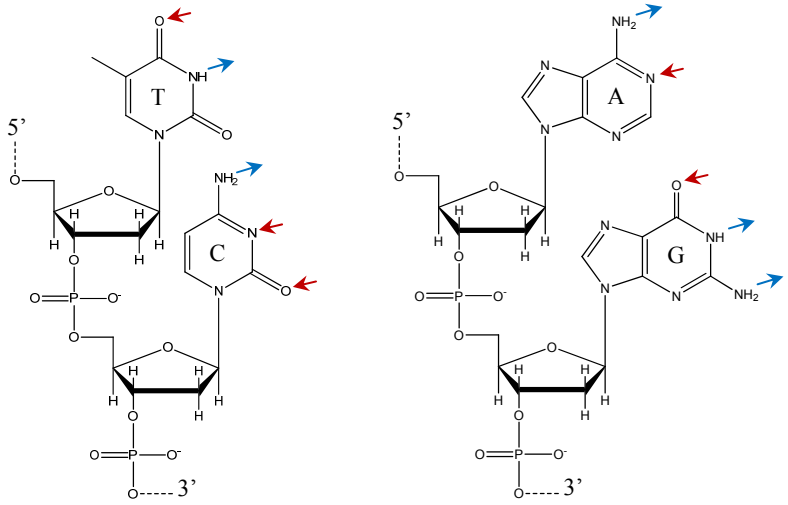

Figure 2.2. The structure of DNA illustrated by the sugar-phosphate backbone and the four bases: thymine (T), cytosine (C), adenine (A), and guanine (G). The pattern of hydrogen binding is the mechanism behind specific base pairing between A and T, and between C and G. Hydrogen bond donating and accepting groups highlighted by arrows.

Unlike the unordered ssDNA coil, dsDNA can adapt several distinct conformations, some of which are illustrated in Figure 2.3. The familiar double helix prevalent at physiological conditions is known as B-DNA. Biological significance is also assigned to A-DNA and Z-

DNA, two alternative DNA conformations which require specific conditions to remain stable.[14] Finally, B-DNA is converted into Psi-DNA in the presence of neutral or cationic macropolymers at high salt concentration.[15] While Z-DNA has the opposite helix twist compared to A- or B-DNA, the base pairs are stacked in parallel along the helix axis in all three conformations, and the phosphate backbones face outwards into the surrounding aqueous environment.

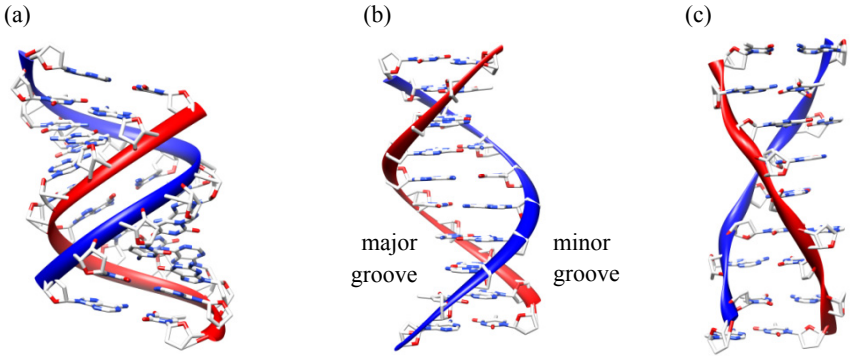

Figure 2.3. The a) A-, b) B-, and c) Z-conformations of DNA. The major and minor grooves in B-DNA are indicated. The structure of Psi-DNA is not known in detail, but its CD spectrum resembles B-DNA more than the other conformations. Structures obtained from Hyperchem nucleic acids database.

2.1 Factors governing dsDNA stability

The structure of B-DNA is well established, but there is considerable disagreement in its thermodynamic properties. Often, the observed stability is explained using four main effects, the two constructive being transversal hydrogen bonding between base pairs and longitudinal base stacking, and the two destructive being electrostatic repulsion between phosphate groups and the entropic difference between one ordered helix and two random coils.[14]

The double helix is traditionally regarded as two strands joined by hydrogen bonds.[16] Bond enthalpies of an AT and a GC pair are often quoted as –12 and –21 kcal/mol, the values justified experimentally as well as theoretically.[17] Formamide and urea efficiently compete with hydrogen bonding between bases and are often used as denaturizing agents to fully separate the two dsDNA strands. However, recent research has proposed a completely different view regarding a DNA molecule in aqueous solution. Water molecules, which act as hydrogen bond donors and acceptors, cause base pairing between C and G to have zero free energy, and base pairing between A and T to be slightly destabilizing.[18-19]

The results above emphasize the importance of base stacking, a collective term for several stabilizing forces in B-DNA due to the parallel arrangement of bases along the helix. Stacking is sometimes partitioned into the hydrophobic effect from burying hydrophobic bases in the helix interior shielded from water molecules, aromatic stacking between overlapping π-orbitals of a base and adjacent bases, electrostatic attractions between minor localized charges, and other minor contributions such as dispersion forces. Although the

effect has been demonstrated both in small molecules[14,20] and with non-natural DNA bases[21-22], stacking free energy has no generally accepted sign or value[14,23]. Using synthetic DNA bases with extra hydrogen binding capability or additional aromatic rings, it was found that hydrogen binding was unaffected and stacking effects decreased by the presence of organic solvents like dioxane or dimethylformamide, leading to an overall decrease in duplex stability.[21,24] However, there was no simple correlation between the degree of destabilization and the structure and properties of the solvents.

In aqueous solution, the strongly anionic phosphate backbones collect a surrounding cloud of cations to achieve overall charge neutrality. Cations will partially shield the electrostatic repulsion between DNA strands, but in addition to pure coulomb forces, the ion composition can be important. For example, the organic polyamine spermine[25] and hydrated magnesium ions[26] stabilize DNA through favorable hydrogen bonds, while copper(II) ions have a denaturizing effect[27].

Finally, the degree of DNA denaturation depends on temperature. Most dsDNA is stable at ambient temperature. At physiological temperature however, many short dsDNA oligonucleotides begin to dissociate, or melt. Raised temperature and increased molecular kinetic energy will eventually lead to complete melting at the melting temperature T_m, a direct measurement of double helix stability. It is possible to calculate T_m approximately by knowing the base sequence using the nearest neighbor method, which assigns a thermodynamic parameter to every two bases. However, these parameters are seldom mechanistically justified or agreed upon.[28-30]

2.2 Breathing and base flipping

In terms of intracellular activity, dsDNA is the inactive form compared to ssDNA. The information storing bases are buried in the helix interior and not easily accessed from outside. Some small molecules[31] as well as polypeptides[32] show sequence specificity by recognizing bases from the sides through the major and minor grooves. However, enzymes catalyzing major events like DNA synthesis and transcription, as well as homologous recombination, require ssDNA.[33]

Under ambient thermal conditions, the double helix unwinds locally into bubbles of single strands with a lifetime of about 50 μs; a spontaneous process called DNA breathing. This can be predicted using theoretical models, but the transient nature is debated.[34-37] DNA breathing is facilitated by end effects in short oligonucleotides, so called end fraying, and has been found to enhance both flexibility and instability of the double helix.[38]

Another particularly transient mode of double helix opening is the outward rotation of a single DNA base which completely breaks two planes of stacking and the hydrogen bonds between a base pair. It is uncertain if base flipping is spontaneous, or if enzyme activity is required.[39-41] Evidence for base flipping was first found in crystallographic images of DNA-methyltransferase complexes, but its time scale in aqueous solution is subject of debate.[42-44] Base flipping is commonly believed to provide nucleation sites for single stranded bubbles, since the interstrand attractive forces are significantly weakened.[45-46]

3 Strand exchange

In living cells, homologous recombination is triggered by the existence of a single strand as a result of targeted or accidental DNA degradation. The single strand is coated with RecA or Rad51 and diffuses into the vicinity of a double helix with the same or similar base sequence. After initiation mechanisms not yet well understood, the single strand probes for its correct position, the original double strand dissociates, and a new double strand and a new single strand are created.

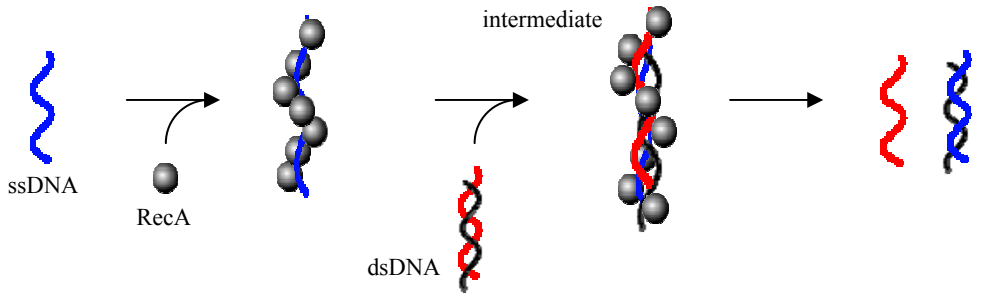

Figure 3.1. Cartoon image of RecA promoted DNA strand exchange. The DNA-protein filament is assembled in two steps, while actual strand exchange occurs in the last step. How dsDNA enters the filament, and the structure of the intermediate, are unknown.

The structures of DNA-RecA and DNA-Rad51 filaments have only recently been described in some detail using a "beads on a string" model, where individual proteins cover the central DNA molecule in a repetitive helical pattern.[5-6] The overall catalytic mechanism currently proposed and accepted by most scientists is that the single DNA strand is restricted in motion, stretched, and forced to adapt a structure similar to the final B-DNA helix. This exposes its nucleotide bases to the incoming complementary strand, which was previously bound to a secondary site on the protein, and facilitates sequence recognition through selective hydrogen binding.[5,47-48]

Enzymatic activity of recombinases *in vivo* is influenced by the intracellular matrix and several other proteins, and requires the presence of Mg^{2+} ions and ATP as well as precise temperature and pH.[7-9,49-50] These conditions must be replicated and remain constant for *in vitro* kinetic studies, which can be difficult to achieve. Therefore, strand exchange is normally assessed *in vitro* using *a posteriori* methods like electrophoresis or by observing the disappearance of ATP, and very little kinetic data is available.

3.1 Thermodynamics of strand exchange

A difference between *in vivo* and *in vitro* DNA strand exchange is the use of short and defined synthetic DNA strands *in vitro*, which eliminates any complications arising from DNA strands of unequal length or sequence. It is easily realized that the thermodynamic properties of reactants and products are identical, so strand exchange is only kinetically limited. In terms of free energy, catalysis is achieved either through simultaneously increasing the reactant and product free energies, or lowering the energy barrier by stabilizing the intermediate product.

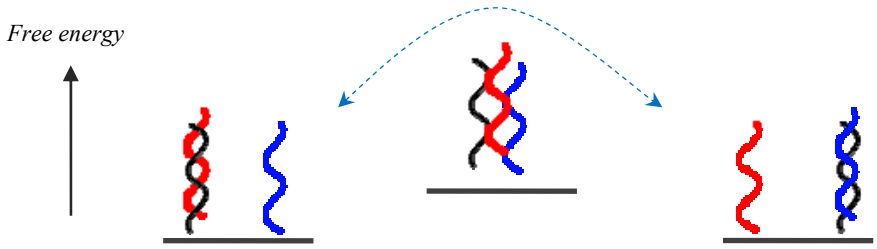

Figure 3.2. Free energy map of strand exchange. The overall free energy does not change, but sterical hindrance, electrostatic repulsion, and decreased entropy create an activation energy barrier.

If the intermediate product of strand exchange were three single strands, selectively stabilizing ssDNA would decrease the energy barrier. However, this assumption is not realistic for long naturally occurring DNA strands.[51] According to recent *in vitro* research, strand exchange at temperatures far from proceeds sequentially through migration of the exchange junction also in short strands.[52-53] Two reasonable models of the intermediate have been proposed: local single stranded bubbles at higher temperatures, or a DNA triplex through nonstandard base pairing at lower temperatures.[13,54]

3.2 Artificial catalytic systems

Existing research into artificial strand exchange has focused on the importance of electrostatic attraction. Large polyarginines, strongly basic polypeptides containing the amino acid arginine, have been demonstrated to accelerate DNA strand exchange with an effect inversely related to salt concentration. By contrast, the equally charged polypeptide polylysine has a much lower activity, which was explained by stronger arginine-DNA hydrogen bonds.[12,55]

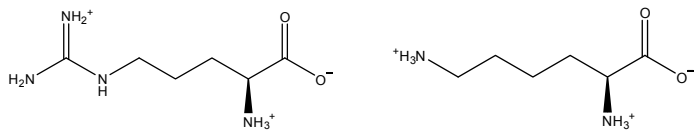

Figure 3.3. Zwitterionic structures for arginine (left) and lysine (right). The guanidine group on the side chain of arginine and the amino group on the side chain of lysine are normally protonated in aqueous solutions.

The concept of using polypeptides has been refined by adding grafted chains of dextran to a charged polylysine backbone. These synthetic polymers are thought to act through a combination of electrostatic interactions and hydrogen binding. The exact mechanism is somewhat unclear, since small changes in polymer structure causes the catalytic activity to disappear, but the many positive charges have been found to promote the formation of DNA triplexes through electrostatic shielding.[13,56] The addition of guanidine groups to mimic the structure of arginine further increased the rate of strand exchange, which also reflects the difference between the two amino acids.[13,52,57]

Another way of approaching charge based catalysis is the use of positively charged liposomes which accelerate DNA strand exchange on the surface.[11,53] The proposed mechanism, in addition to enhanced end fraying, is concentration of DNA from bulk through electrostatic attraction in combination with the effect from two-dimensional alignment of DNA strands as opposed to random three-dimensional orientation. A complicating factor of using DOTAP liposomes is their tendency to quickly aggregate upon addition of DNA. Adding a small amount of PEG chains prevented aggregation, but strand exchange became significantly slower. It can thus not be excluded that charges in combination with the geometry of aggregated liposomes, rather than charges alone, is responsible for much of the activity.

4 Crowding and volume exclusion

The intracellular matrix contains up to 40% macromolecules by weight, resulting in a crowded environment often neglected in studies of biomolecules. The excluded volume depends nonlinearly on molecular size and concentration, and is always larger than the net occupied volume (see Figure 4.1). Since less space is available per molecule, the effective concentration of any given solute is significantly higher than its nominal concentration.[58-60] It has been shown that crowding increases the stability of proteins due to sterical reasons[61], and that diffusion is strongly limited in crowded environments[62-63].

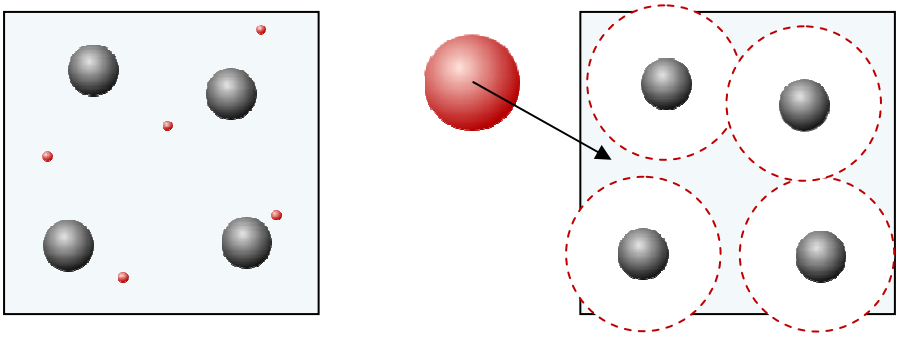

Figure 4.1. The excluded volume depends on molecular size. A small solute (red dots) can exist anywhere in the enclosed area despite the presence of crowding agents (black spheres), but the volume available to the center of a larger solute (red sphere) is very limited due to sterical hindrance. Radius of red dotted circles is the sum of radii of red and black spheres.

4.1 Macromolecular polymers

Dextran and polyethylene glycol (PEG) are two inert biocompatible macropolymers frequently used to simulate crowded intracellular conditions. Especially PEG has been found to occupy a much larger volume than would be expected from its formula alone (structures of dextran and PEG are presented in Figure 6.1). Therefore, other macromolecules are effectively excluded from a PEG solution. A famous example is the PEG-dextran-water system which forms separate PEG and dextran phases, although both phases are aqueous.[64-66] Furthermore, activity of RecA is enhanced by the presence of 10% PEG or polyvinyl alcohol (PVA) by weight-volume ratio. It was proposed that the presence of PEG or PVA acts indirectly by allowing formation of DNA-protein complexes at otherwise insufficient Mg^{2+} concentrations.[49]

Dextran is water soluble due to its many hydroxyl groups, but concentrated solutions of dextran, like other carbohydrates, are highly viscous. On the other hand, PEG is nonpolar but still highly water soluble, while its two analogs polymethylene glycol and polypropylene glycol are insoluble. This is often explained by the special arrangement of water molecules

around a PEG chain, making the distance between two adjacent ether oxygen atoms important.[67-69]

PEG can selectively destabilize a DNA duplex while stabilizing a DNA triplex, which has been explained by the greater number of water molecules associated with a duplex.[70] Addition of PEG decreases bulk water activity[71], and the duplex was thought to be sensitive to such dehydration. However, the triplex stabilization was not explained.

An alternative view is presented by studies which show that short PEG chains and PEG at high concentrations destabilize DNA, while longer PEG at low concentration has the opposite effect.[72] Though the dependence on PEG length was not explained, it was found that PEG decreases the number of sodium ions needed to stabilize the DNA double helix. This was attributed to a stronger ionic bond between phosphate groups and sodium ions due to decreased bulk dielectric constant.[60,73]

5 Fundamental concepts

This chapter covers kinetic modeling of strand exchange and the basics of a few spectroscopic techniques used to study DNA.

5.1 Kinetic modeling of strand exchange

By tradition, DNA strand exchange is soft modeled using single exponential negative decay kinetics

$$u(t) = -\alpha e^{-k_{obs}t} + \beta \tag{1}$$

with $u(t)$ describing the concentration of the formed duplex, and β as the equilibrium concentration. The model fits to experimental data, and the observed rate constant k_{obs} is quoted as the efficiency or speed of strand exchange.[11,13]

However, there is an important counterexample to the reliability of above presented model. Consider a strand exchange reaction between a double strand AB with the initial concentration $[AB]_0$ and a single strand C of equal length with the initial concentration $[C]_0$. The reaction can be written

$$AB + C \underset{k}{\overset{k}{\rightleftharpoons}} AC + B$$

where B and C has the same sequence, and A has a complementary sequence. In a simplified and ideal case, the reaction is governed by the true first order rate constant k identical for forward and reverse reactions. We thus obtain for the desired product AC

$$\frac{d[AC]}{dt} = k[AB][C] - k[AC][B] \tag{2}$$

and this becomes

$$\frac{d[AC]}{dt} = k([AB]_0 - [AC])([C]_0 - [AC]) - k[AC]^2 \tag{3}$$

since $[AB] = [AB]_0 - [AC]$, $[C] = [C]_0 - [AC]$, and $[B] = [AC]$. After cancelling quadratic terms, (3) simplifies to a first order ordinary differential equation:

$$\frac{d[AC]}{dt} = -k([AB]_0 + [C]_0)[AC] + k[AB]_0[C]_0. \tag{4}$$

Equation (4) is easily solved using the boundary condition $[AC] = 0$ for $t = 0$ and we finally obtain

$$[AC](t) = -\frac{[AB]_0[C]_0}{[AB]_0 + [C]_0} e^{-k([AB]_0+[C]_0)t} + \frac{[AB]_0[C]_0}{[AB]_0 + [C]_0}. \tag{5}$$

Comparing expressions (1) and (5), we conclude that

$$k_{obs} = k([AB]_0 + [C]_0) \tag{6}$$

which shows that the observed rate constant differs considerably from the true rate constant, and actually depends on initial DNA concentrations.

5.2 Absorption and emission

According to the wave-particle duality principle, propagating electromagnetic waves of light can also be described as travelling in discrete quanta sometimes referred to as photons. If the difference ΔE between two energy states of a molecule satisfies the Bohr frequency condition

$$\Delta E = h\nu = \frac{hc}{\lambda}$$

where h is Planck's constant and c is the speed of light, a photon with frequency ν or wavelength λ may be absorbed and the molecule is excited to the higher energy state. Absorption is conveniently defined as the logarithm of the ratio between incident and transmitted light, or

$$A = \log_{10} \frac{I_0}{I}.$$

A melting curve is absorbance plotted against temperature to visualize the interdependency. Melting curves of DNA are especially useful, since the transition of double stranded DNA into single stranded DNA is accompanied by an increase in absorbance, also known as hyperchromic effect. The temperature at the maximum derivative of the melting curve is defined as the melting temperature T_m. Well above and well below T_m, the sample contains only single strands or only double strands. It is possible to calculate the enthalpy and entropy of strand dissociation from melting curves using several methods[24], however, those calculations are for the time being out of the scope of this study.

When promoted by a photon to a higher electronic state, some species called fluorophores may return to the ground state by emitting a new photon, a phenomenon known as fluorescence when occurring between singlet states, or phosphorescence if involving a triplet state. Energy is lost in the process due to Stokes' shift and due to a quantum yield less than unity, both of which depend on the local fluorophore environment.

5.3 Circular dichroism

To study the chiralness of molecules and, as a specific example, the conformation of DNA, absorbance can be measured using alternately left and right circularly polarized light. Circular dichroism (CD) is then calculated as the difference in absorbance:

$$CD = A_L - A_R.$$

CD is zero for achiral or racemic samples due to symmetry, and an enantiomerically pure sample will produce the mirror CD spectrum of the other enantiomer. DNA is chiral, and thus has a non-zero CD spectrum, the shape of which is determined by its conformation. The CD spectra of the major forms of DNA are presented in Table 1.

Table 1. CD spectra of DNA conformations.

conformation	**CD at wavelength**		
	~240 nm	**~260 nm**	**~280 nm**
A-DNA[14]	weakly negative	strongly positive	strongly positive
B-DNA[14]	negative	zero	positive
Z-DNA[14]	positive	positive	negative
Psi-DNA[74]		negative	negative

5.4 FRET spectroscopy

Förster resonance energy transfer (FRET) is the major technique used in this study to trace the kinetics of DNA strand exchange. FRET occurs when an excited fluorophore transfers its energy to a second molecule, and is thus a special case of quenching. Though the emission spectrum of the energy donor must overlap the absorption spectrum of the acceptor, the transfer is due to dipole-dipole coupling and completely nonradiative.

FRET is very distance-dependent. The FRET quantum yield E, which is the ratio between photons absorbed and energy transfer events occurred, can be expressed as

$$E = \frac{1}{1 + \left(\frac{r}{R_0}\right)^6}$$

where r is the distance between fluorophores and R_0 is the so called Förster distance which depends on the fluorophores and their mutual orientation but is normally in the range of 2-6 nm[75]. The inverse sixth power expresses the rapid decline of FRET efficiency, which allows its use as a binary on-off probe.

6 Materials and methods

DNA oligonucleotides with and without 5' FAM or 3' TAMRA fluorophore modification, presented in Table 2, were purchased from ATDbio. The mismatched M strand was a gift from Jonas Hannestad. Double stranded DNA was prepared by heating single strands to 90°C and slowly annealing over 6 hours. Experiments were performed in PBS buffer (50 mM sodium phosphate, pH 7.5, 1 mM EDTA) with NaCl added to desired Na^+ concentration.

Table 2. Oligonucleotide sequences with and without fluorophore modification, mismatches relative to O_1 are highlighted in red.

abbreviation	sequence
O_1	3′-GCA GTT GTA TGT ATA GTG GT-5′
O_2	3′-GCA GTT GTA TGT ATA GTG GT-5′-FAM
O_3	5′-CGT CAA CAT ACA TAT CAC CA-3′
O_4	5′-CGT CAA CAT ACA TAT CAC CA-3′-TAMRA
m_4	5′-CGT **A**AA CAT ACA TAT CAC CA-3′-TAMRA
m_5	5′-CGT C**C**A CAT ACA TAT CAC CA-3′-TAMRA
m_{10}	5′-CGT CAA CAT **C**CA TAT CAC CA-3′-TAMRA
M	5′-**A**GT CA**C** **TA****A** **T**CA **GTA** C**GT** C**T**-3′

Peptides were used to investigate the importance of charges to the strand exchange reaction. The amino acids arginine and lysine were selected according to previous studies, but the total polypeptide charge and the charge density were reduced. The peptides, presented in Table 3, were a gift from Shugang Zhang, except for R7 which was purchased from Innovagen. Purity of the synthesized peptides was assessed using analytical HPLC and no serious contamination or degradation was found.

Table 3. Peptide sequences with terminal modifications.

abbreviation	sequence
KL	Ac-WWKK-WWKK-WWKK-WWKK-CONH
KS	Ac-WWWKK-CONH
RL	Ac-WWRR-WWRR-WWRR-WWRR-CONH
RS	Ac-WWWRR-CONH
R7	H_3N-WRRR-RRRR-CONH

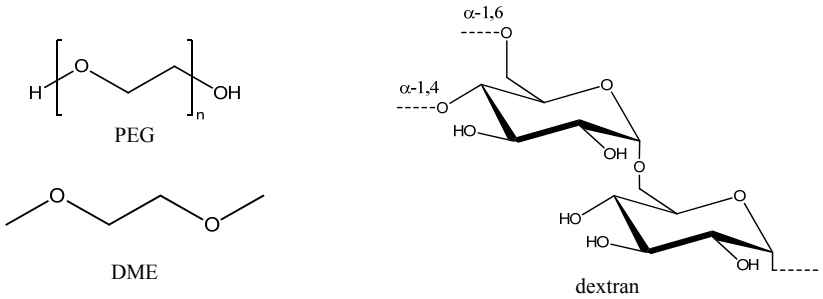

Figure 6.1. The structures of PEG, DME, and dextran. Dextran is a branched polysaccharide composed of hexose units, while PEG and DME are ethers.

Dextran T500 (approximate degree of polymerization is 500) from Pharmacia and PEG from BDH with a molecular weight between 5000 and 7000 were used as crowding agents to study the effect of volume exclusion. Dextran and PEG solutions were made by mixing an appropriate amount of polymers and 15 mL PBS buffer with 50 or 200 mM Na^+ in a conical centrifugation tube with slow over the end rotation for at least 60 minutes. The solutions were allowed to equilibrate in room temperature for 1 week before use. In this thesis, all PEG concentrations are expressed in weight percent.

Dimethoxyethane (DME), kindly provided by Nina Kann, was used as a monomeric analog to PEG. Unlike ethylene glycol, a diol used in several earlier studies of PEG, DME contains the same functional units and has the same distance between its oxygens.

6.1 Instrumentation

Concentrations of oligonucleotides and peptides were determined through absorbance measurement using a Thermo Scientific Nanodrop 1000 spectrophotometer, with at least four measurements averaged. Absorption spectra and melting curves of DNA were obtained using a multicell thermoregulator equipped Varian Cary 4000 UV-Vis spectrophotometer with 1.5 mL reduced volume quartz absorption cells; amount of substance of dsDNA was 0.5 nmol.

Fluorescence spectra and kinetics were measured on a multicell thermoregulator equipped Varian Cary Eclipse fluorometer with 1.5 mL reduced volume quartz fluorescence cells. Dynamic light scattering was measured using a Malvern Zetasizer with disposable polystyrene cells. CD was measured on a Jasco J-810 Spectropolarimeter with a step size of 1 nm, response time 30 seconds, and 8 runs were averaged; amount of substance of dsDNA was 50 nmol, the same as for melting curve measurements.

6.2 Liposomes and immobilized peptides

Liposomes and beads are two morphologically equivalent scaffolds for the assembly of positive charges into a spherical catalytic surface. The lipids DOPC and DOPG were from Larodan, DOTAP from Sigma, and DSPE-MPEG from Biotrend. According to the published procedure[11], lipids were dissolved and mixed in chloroform. Solvent was then removed through rotary evaporation and overnight vacuum. After adding PBS buffer and vortexing for 20 minutes, the liposomes were frozen five times in liquid nitrogen and heated to 45°C in

between and the last time slowly thawed at room temperature. Lastly, the liposomes were extruded 21 times through a 100 nm filter using a hand held extruder. The quality was assessed using dynamic light scattering, with the Z-average size maintained between 105 and 115 nm.

Cationic liposomes were composed of zwitterionic DOPC and 35% cationic DOTAP, while cationic liposomes with PEG had 3% of DOPC replaced by DSPE-MPEG. Since half of the charged DOTAP head groups face inwards, the effective surface charge used in this thesis is half the nominal charge. Anionic liposomes had 35% anionic DOPG in addition to DOPC, and enough R7 was added to achieve a surface charge equivalent to the cationic liposomes.

Peptides were immobilized using carbodiimide coupling chemistry on 1 µm Invitrogen Dynabeads Myone with carboxylic acid surface groups according to the instructions provided by the manufacturer. The procedure is outlined in Appendix 2.

6.3 Kinetic traces

To record kinetic traces of DNA strand exchange, O_3 in 5 times excess was added to the duplex O_2O_4 (or O_2m_x for experiments with mismatched strands), in which FAM and TAMRA constitute an energy transfer pair. Upon strand exchange, the new O_2O_3 duplex is formed and FAM emission is recovered (see Figure 6.2). Additionally, FAM in O_2O_3 has a different fluorescence than in O_2, which shows that actual FAM emission may depend on its DNA environment. Emission spectra of individual strands, in addition to those in Chapter 7, are found in Appendix 1.

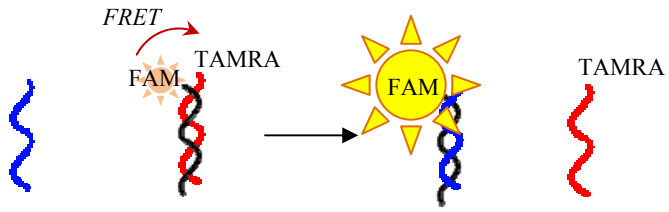

Figure 6.2. The principle behind emission recovery of FAM due to strand exchange. The O_2 (black)/O_4 (red) duplex forms a FRET pair, quenching FAM emission until the TAMRA-modified O_4 strand is displaced by unlabeled O_3 (blue).

For kinetic measurements in non-viscous buffers, liposomes, peptides, and dsDNA were added in that order to a cell with twenty inversions between each step. Initial fluorescence was monitored for at least 20 minutes until no change could be observed, ssDNA was quickly added, and the sample was inverted twenty times. For viscous samples containing dextran or PEG, polymer solution and dsDNA were vortexed in an eppendorf tube and preheated to desired temperature before ssDNA was added. The sample was then vortexed for 10 seconds, transferred to a cell, and inserted into the fluorometer. Initial fluorescence was measured using a separate sample.

Unless otherwise stated, recovery of FAM fluorescence was monitored at the emission maximum of 517 nm using excitation wavelength 496 nm, with a 10 nm excitation slit and a 5 nm emission slit. The photomultiplicator potential was set at 600-800 V to maintain a raw signal between 50 and 1000. Final volumes for all samples were 1 mL, the amount of substance of dsDNA duplex was 14.4 pmol, and the amount of substance of ssDNA was 72 pmol. The dilution effect of 1% on initial fluorescence due to addition of ssDNA was ignored. Yield was computed using

$$yield(t) = \frac{FI(t) - FI_0}{FI_\infty - FI_0} \tag{7}$$

where $FI(t)$ refers to the fluorescence intensity of FAM at a certain time, FI_0 is the initial fluorescence before addition of ssDNA, and FI_∞ is the equilibrium fluorescence. In practice, FI_∞ was obtained by measuring a heated and annealed sample containing all three DNA strands, referred to as $O_2O_4 + 5O_3$ matching and $O_2m_x + 5O_3$ for mismatching strands.

Kinetic curves were fitted in Origin 7 SR4 using the built in expression

$$y = y_0 - Ae^{-x/\tau} \tag{8}$$

where τ is the inverted value of k_{obs} from expression (1). The time frame selected for reactions which did not complete was $4 \cdot 10^4$ seconds in PEG solutions and 10^4 seconds in the presence of peptides.

6.4 Molecular modeling

Protein structures were visualized using UCSF Chimera alpha version 1.3, which was also used to assign amino acid residues as hydrophobic or charged. Molecular dynamics were simulated with Hyperchem Professional 7.52. Structures of polypeptides and DNA were created using the built in amino acids and nucleic acids database, DNA as B-DNA, and polypeptides as β-sheets. Using the AMBER molecular mechanics force field (distant dependent ε with scale factor 1, electrostatic and van der Waals scale factors 0.5, no cutoff), the polypeptide and DNA structures were optimized separately to an RMS gradient of 0.01 kcal/(Å·mol), added together, and optimized again to 0.001 kcal/(Å mol). Polypeptide binding was assessed after a 1 ns molecular dynamics simulation at 290 K, since longer simulations were not more informative.

7 Results

In this chapter the results from the studied model systems are presented. First the molecular modeling of peptide-DNA interaction is presented, followed by strand exchange catalysis by free and immobilized peptides. Finally the results from the studies of molecular crowding by PEG, DME, and dextran are given. Some additional information is presented in the appendix.

7.1 Interactions between DNA and peptides

The crystallographic image of a RecA-ssDNA filament shows a central ssDNA strand almost entirely surrounded by RecA monomers in a helical pattern (see Figure 7.1).

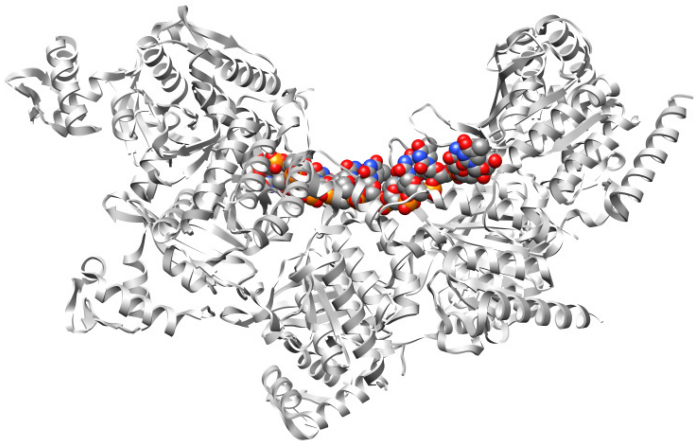

Figure 7.1. Cartoon rendering of a short section of single stranded DNA (center) surrounded by five RecA units (grey). Image created from the entry 3CMW in RSCB Protein Data Bank.

The DNA has a stretched conformation, and the so-called L1 loop of the protein is inserted between two bases, disrupting the base stacking interactions. As seen in Figure 7.2, positive charges are localized to the phosphate backbone, while the residues close to the base pairs are hydrophobic. Overall, the elongated inner cavity of the protein filament is a predominantly nonpolar and crowded environment. There is approximately one positive charge per phosphate when bound to ssDNA, but only one third of a charge when bound to a three stranded intermediate.

To further investigate the importance of charged amino acids, molecular simulations were performed with dsDNA and either four diarginines or one octaarginine, or solely DNA as negative control. When arginines were initially positioned in certain ways relative to DNA, the two positive charges of diarginine were attracted to the same DNA strand, and DNA distortions were minimal. When diarginine and octaarginine successfully bound to both strands, the free DNA ends were bent and distorted, and the whole helix somewhat compacted (see Figure 7.3). Polyarginines were found in the simulations to have a favorable mode of DNA binding, with the peptide backbone residing in the major groove, and the side chains bound to the phosphate groups of either strand.

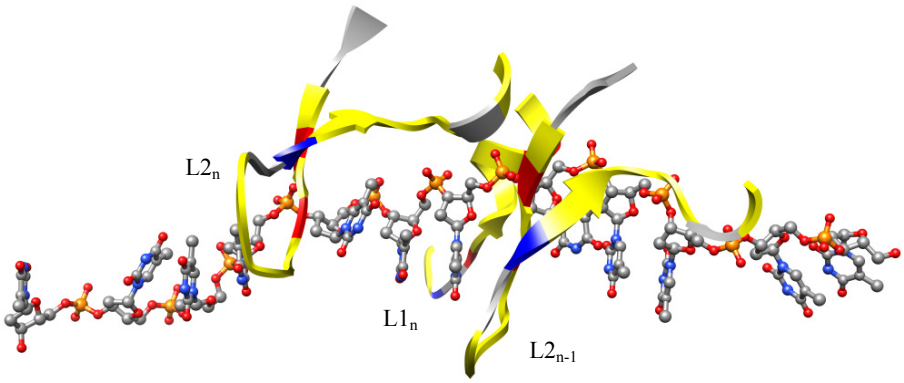

Figure 7.2. Interactions between DNA and the RecA L1 and L2 loops. The L1 loop of one unit cooperates with the L2 loop in the previous unit to partition DNA into segments of three nucleotide bases. Hydrophobic amino acid residues in yellow, positive and negatively charged residues in red and blue, respectively.

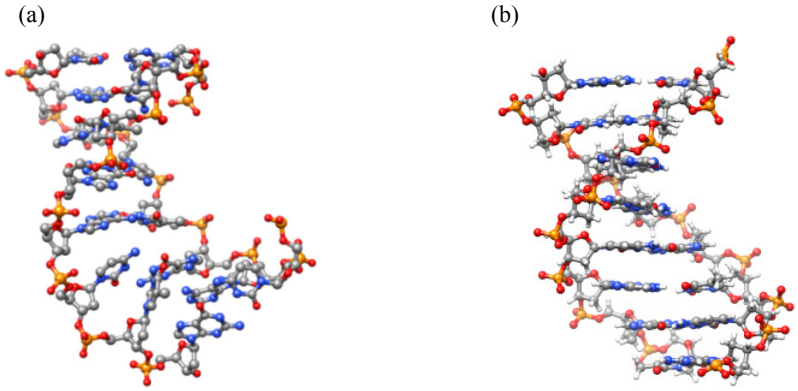

Figure 7.3. a) Out of plane bending and distortion of the double helix with sequence ATCG ATCG by a major groove bound octaarginine (not shown for clarity) after 1 ns of simulation. b) DNA in the absence of arginine after 1 ns of simulation.

Both protein structure and molecular modeling suggest that a few positive charges may be sufficient for peptide-DNA interactions. To study this experimentally, melting curves of the DNA duplex O_1O_3 in presence of the lightly charged polypeptides RS and KS (see Table 3), the longer polypeptides RL and KL with dispersed charges, and the short polyarginine R7 were obtained as presented in Figure 7.4. Peptides affected neither the melting temperature nor the shape of the melting curves, with the exception of R7 which increased T_m by approximately 10ºC at higher concentrations. The melting curves with R7 displayed an initial negative slope due to the peptide, which was not reversible after cooling and subsequent heating.

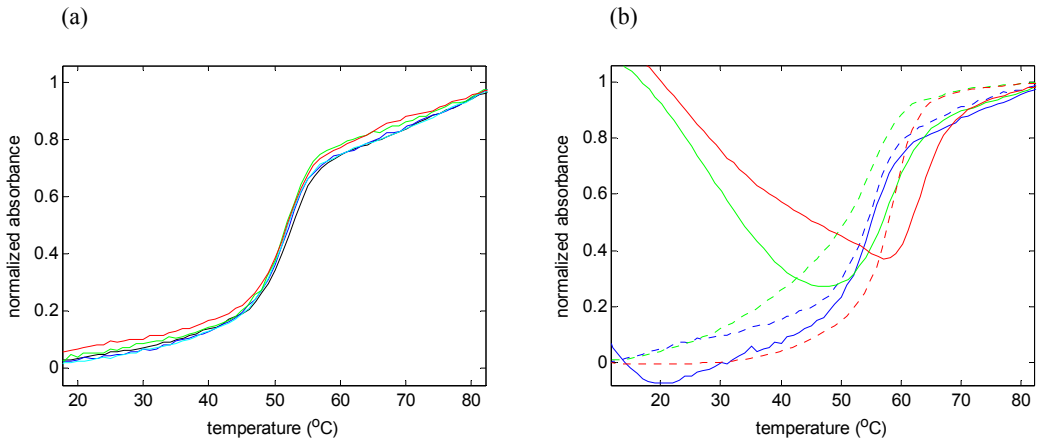

Figure 7.4. Melting curves of DNA in the presence of peptides. a) DNA (black), RL (blue), RS (cyan), KL (green), and KS (red), all with peptide:DNA charge ratio of 5.0. All T_m are 52ºC. b) R7 with peptide:DNA charge ratio 0.5 (blue), 1.0 (green), and 2.0 (red). Solid lines indicate heating and dotted lines cooling. T_m for heating and cooling are 54/55ºC, 58/56ºC, and 63/59ºC respectively.

As expected, fluorescence emission from O_2O_4 was unchanged by the four peptides which did not affect T_m (see Figure 7.5a). FAM emission was steadily quenched when R7 was added. It is not known if this is due to compaction of DNA and decreased distance between FAM and TAMRA, or collision quenching from the tryptophan residue on R7. However, TAMRA emission initially increased to a maximum at a peptide:DNA charge ratio of 1, returned to the base level at a ratio of 2, and then rapidly declined when the ratio was increased to 3 (see Figure 7.5b).

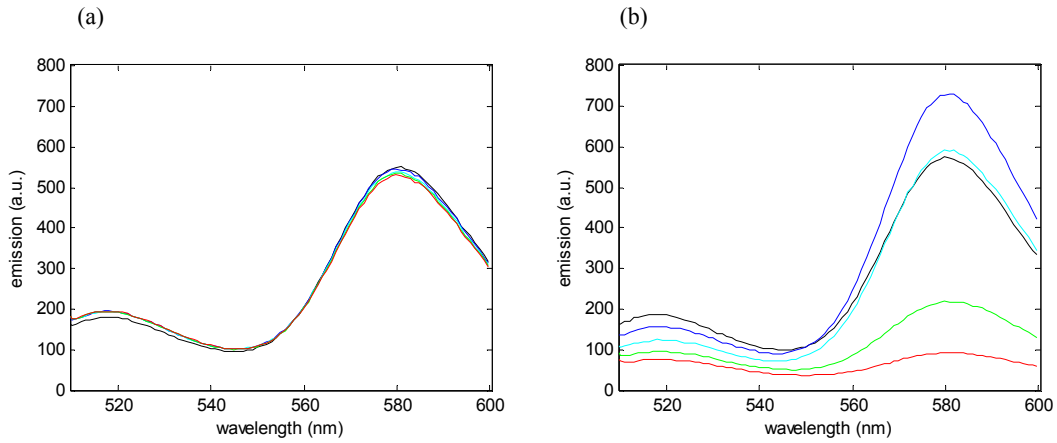

Figure 7.5. Emission of O_2O_4 excited at 496 nm in the presence of peptides at 24°C. The peak at 517 nm is due to FAM and at 580 nm due to TAMRA. a) RL with peptide:DNA charge ratio of 0.0 (black), 1.0 (blue), 2.0 (cyan), 2.6 (green), and 3.2 (red). b) R7 with peptide:DNA charge ratio of 0.0 (black), 1.0 (blue), 2.0 (cyan), 2.6 (green), and 3.2 (red).

7.2 Peptide catalyzed strand exchange

While strand exchange in presence of several peptides were studied at various salt concentrations between 50 and 300 mM Na^+, only R7 possessed clear catalytic activity (see Figure 7.6). However, catalysis is strongly dependent on peptide concentration. For low peptide:dsDNA charge ratios, yields increase with peptide concentration. At a higher ratio than 1, yields significantly decrease and are also negatively correlated to the absolute peptide concentration. Although reaction rates do not exhibit the same clear trend, low yields are associated with larger rate constants (see Table 4).

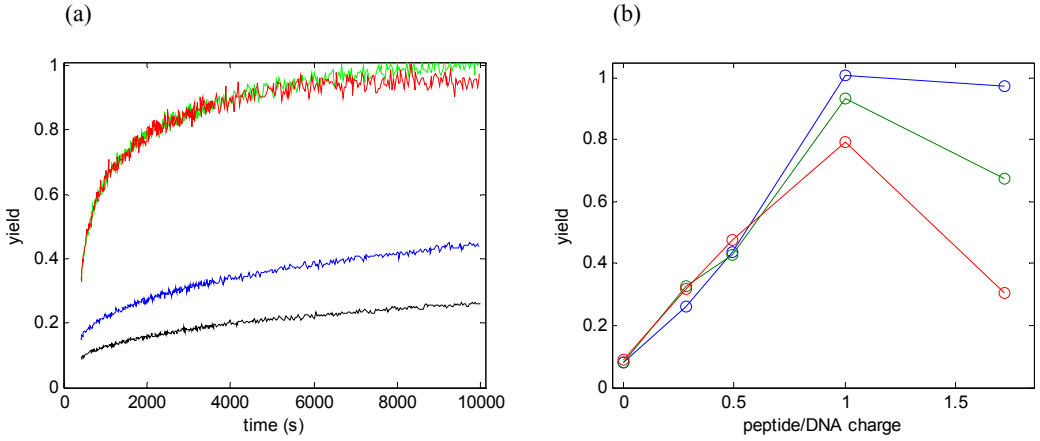

Figure 7.6. Strand exchange in the presence of R7 at 24°C and 50 mM Na^+. a) Kinetic traces of strand exchange with peptide:dsDNA charge ratio 0.28 (black), 0.49 (blue), 1.00 (green), and 1.72 (red). b) Observed exchange yields at 10^4 s with 1.44 (blue), 2.88 (green), and 5.76 (red) pmol dsDNA.

Table 4. Fitted parameters according to model (8) for strand exchange using R7, with a time frame of 10^4 seconds.

dsDNA concentration (pmol)	**peptide:DNA charge ratio**	**fitted parameters**		
		$y_0{}^a$	A	τ
14.4	**0.00**	0,082	0,051	3317
	0.28	0,280	0,223	4758
	0.49	0,460	0,348	4405
	1.00	1,128	0,771	1754
	1.72	0,961	0,661	1430
28.8	**0.00**	0,085	0,055	3652
	0.28	0,356	0,284	4791
	0.49	0,429	0,313	3297
	1.00	0,936	0,652	2905
	1.72	0,683	0,548	3150

57.6	**0.00**	0,093	0,063	3896
	0.28	0,326	0,254	3874
	0.49	0,468	0,332	3176
	1.00	0,806	0,599	2947
	1.72	0,297	0,176	702

[a] Kinetic traces with y_0 differing from 1 did not fit well using model (1).

To create a two-dimensional catalytic surface mimicking DOTAP liposomes which accelerate strand exchange[11], R7 was added to the surface of anionic DOPC/DOPG liposomes and compared to DOTAP liposomes with and without 3% DSPE-MPEG. At low liposome concentration, anionic liposomes carrying R7 clearly outperform liposomes with 35% DOTAP (see Figure 7.7a). This is reversed at high liposome concentration, at which the activity of both DOTAP and pegylated liposomes increase greatly, while R7 liposomes are only moderately affected. Using DLS, liposomes with 35% DOTAP were found to quickly aggregate, while liposomes with R7 and pegylated DOTAP liposomes did not.

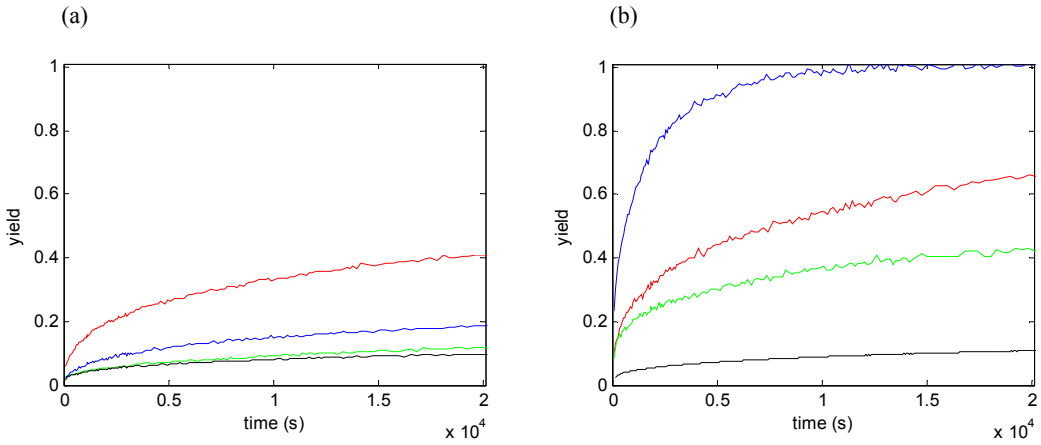

Figure 7.7. Kinetic traces of strand exchange in the presence of liposomes at 24°C, with a) lipid:ssDNA charge ratio 1, and b) lipid:(ss+ds)DNA charge ratio 1. DOPC (black), 65% DOPC + 35% DOTAP (blue), DOPC + DOTAP + 3% DSPE-MPEG (green), and DOPC + 35% DOPG + R7 (red).

Beads were used as another way of immobilizing peptides. Synthesis of R7 coated beads was successful with a yield of over 95%, determined by a material balance of tryptophan established through absorbance measurement of buffers before and after the reaction. Catalytic activity of coated beads could not be proved despite attempts with or without a magnetic stirrer and increasing the number of peptides per bead by one or two magnitudes. The fluorescence signal at 517 nm increased linearly for $2 \cdot 10^5$ seconds without reaching equilibrium (see Figure 7.8a) and without any significant difference between coated and uncoated beads. Figure 7.8b shows the strong scattering from the beads, which at 517 nm is five times the emission from FAM. In the absence of fluorescently labeled DNA, the

fluorescence signal decreased almost linearly due to sedimentation, with a tendency to be lower for coated beads. A good reference value could not be obtained, but the yield after $1 \cdot 10^5$ seconds is in the range of 0.3 to 0.4 after subtraction of the sedimentation baseline.

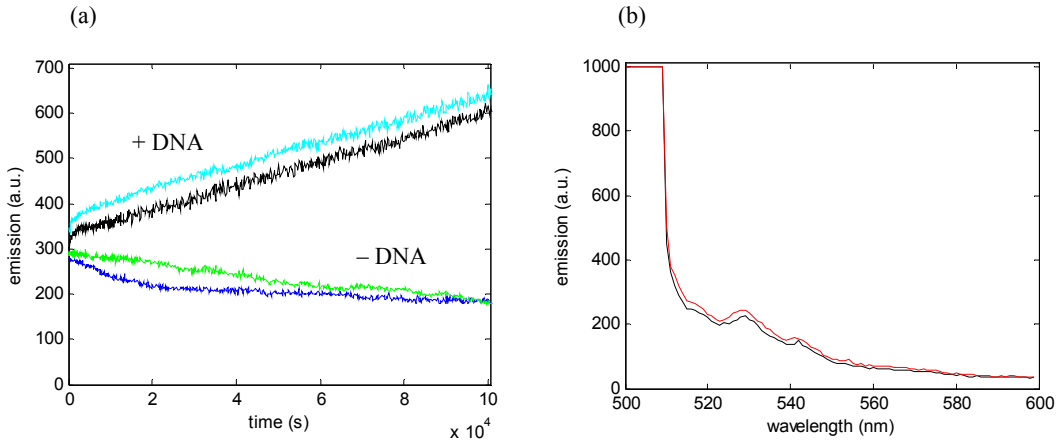

Figure 7.8. a) Typical kinetic traces with magnetic stirring of R7 coated beads (black/blue) and uncoated beads (cyan/green). b) Emission spectra of R7 coated beads (red) and uncoated beads (black) excited at 496 nm.

7.3 DNA in crowded environments

To investigate the properties of PEG solutions, the density was measured at different PEG concentrations in PBS (see Figure 7.9a). The nearly proportional relationship between volume and weight fraction in Figure 7.9b suggests that the PEG-water mixture is approximately ideal, without secondary PEG structures, and with no apparent effects due to close contact between individual PEG chains.

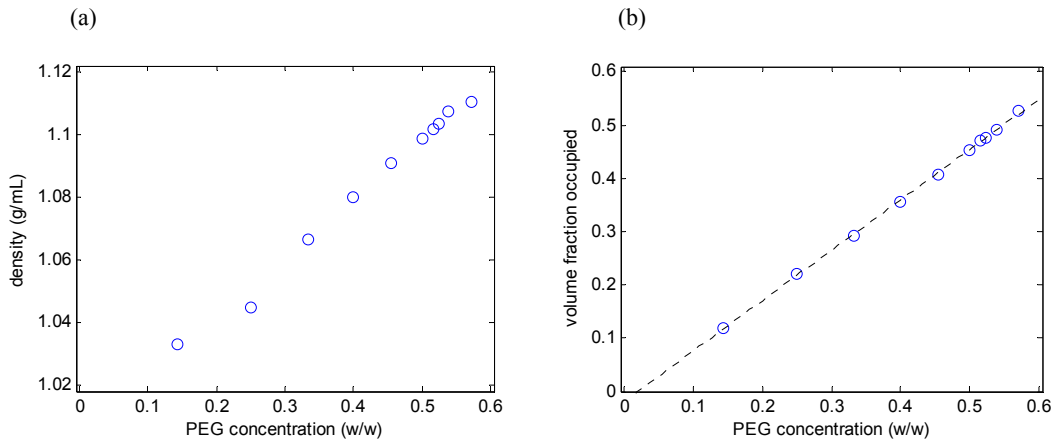

Figure 7.9. a) Measured density of solutions of PEG in PBS buffer indicated by circles. b) Volume fraction occupied by PEG in PBS buffer (circles), calculated from the data in a) by the formula $1 - (V_{PBS} \cdot \text{density})/(m_{PBS} + m_{PEG})$, and the least squares linear interpolation (dotted line).

No hyperchromic shift due to DNA denaturing in the presence of PEG could be detected in the absorption spectra presented in Figure 7.10b. The slightly elevated absorbance at 260 nm in 50.0% PEG could be due to difficulties in handling concentrated PEG solutions, and the shift is very small compared to the almost 50% increase found in melting curves when dsDNA is converted to ssDNA.

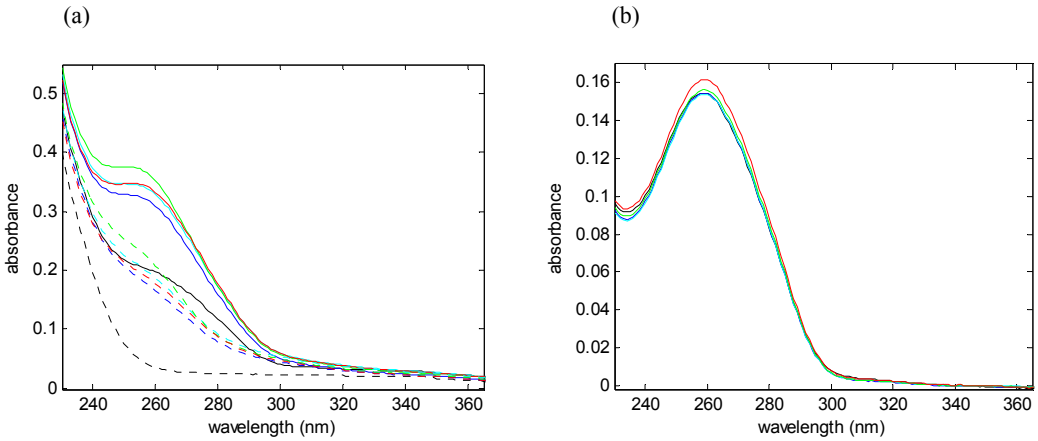

Figure 7.10. Absorption spectra of DNA in PEG solution. a) 0.0% (black), 40.0% (blue), 45.5% (cyan), 47.4% PEG (green), and 50.0% (red) PEG with DNA absent (dotted) or present (solid). b) Baseline corrected absorption spectra of DNA, calculated through pairwise subtraction of the spectra in a). The amount of substance of DNA was 0.5 nmol.

T_m is slightly increased by 40% PEG, and decreased by 50% PEG (see Figure 7.11). Furthermore, since the baselines below 40ºC are flatter in PEG solution than in PBS, the dsDNA-ssDNA transition seems to be better defined with PEG present, and the population of completely intact DNA duplexes is higher at low temperatures. An additional 150 mM Na^+ increased the melting temperatures by approximately 10 degrees for both PBS and PEG solutions, as summarized in Table 5.

Table 5. Melting temperatures of DNA in PEG with ± standard deviation between two replicates with four runs each.

[Na^+]	**% PEG**									
	0.0	±	**40.0**	±	**45.5**	±	**47.4**	±	**50**	±
50 mM	52.0	0.4	53.0	0.6	50.0	0.7	48.2	0.5	46.8	0.6
200 mM	61.0	0.8	61.3	0.6	59.2	0.5	55.5	0.6	54.8	0.9

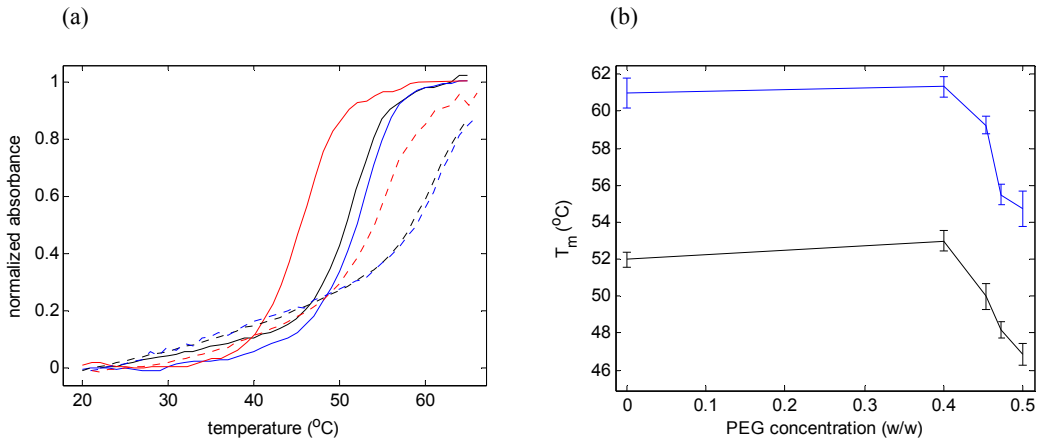

Figure 7.11. Melting curves of DNA in PEG solution. a) 0.0% (black), 40.0% (blue), and 50.0% (red) PEG with 50 mM (solid) or 200 mM (dotted) Na^+. b) T_m with 50 mM (black) or 200 mM (blue) Na^+. Error bars indicate ± standard deviation between two replicates with four runs each.

CD spectra of O_1O_3 have been measured in PBS and 50% PEG at different temperatures (see Figure 7.12) to investigate the DNA conformation in PEG solutions. The results clearly show that a B-DNA conformation is maintained at 24ºC and 37ºC, and that the salt concentration is insufficient to induce a transition to Psi-DNA despite the presence of 50% PEG. As temperature approaches T_m, DNA melting leads to a clear perturbation in the CD spectra, but no obvious trace of ssDNA is visible at 37ºC. The strong CD signal at 220 nm is caused by an unknown contaminant in PEG, also found in CD spectra of PEG dissolved in distilled water (not shown).

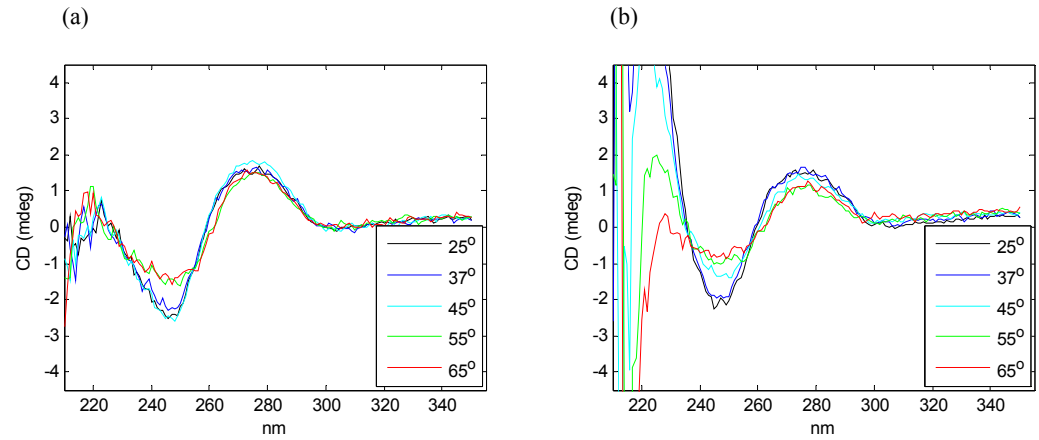

Figure 7.12. CD spectra at different temperatures of DNA in a) absence and b) presence of 50.0% PEG. Amount of substance of DNA was 0.5 nmol, spectra are not normalized.

In PBS, the quantum yield of FAM in O_2O_4 is slightly higher at 37ºC than at 24ºC due to extra thermal kinetic energy and less efficient FRET quenching (see Figure 7.13a). Addition of 50% PEG has two effects: firstly, both FAM and TAMRA fluorescence is increased; secondly, the difference in FAM fluorescence between 24ºC and 37ºC is larger than in PBS, and the difference in emission between and thermally annealed O_2O_4 + $5O_3$ is smaller (see Figure 7.13b). Note that PEG shifts the emission maximum of FAM from 517 nm to 527 nm, indicating a hydrogen bond accepting rather than hydrogen bond donating environment[76]. All kinetic traces of strand exchange in PEG solutions were collected at 527 nm.

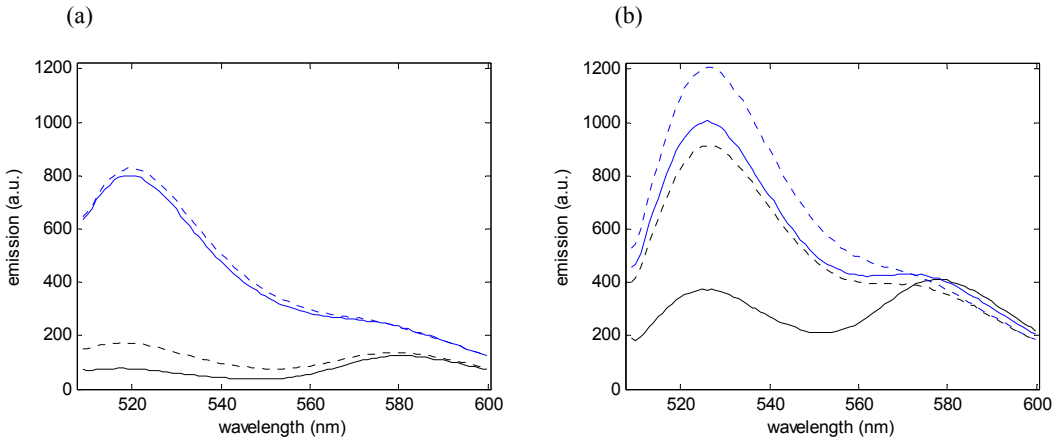

Figure 7.13. Emission of O_2O_4 (black) and O_2O_4 + $5O_3$ (blue) excited at 496 nm in a) absence and b) presence of 50% PEG, with 50 mM Na^+. Solid lines indicate 24ºC and dotted lines 37ºC.

In PBS with 200 mM Na^+, the overall appearance of the spectra remains unchanged, though fluorescence is lowered by increased duplex stability and more effective FRET. Additionally, the difference in FAM signal between O_2O_4 and O_2O_4 + $5O_3$ in PEG solution is larger than in PBS.

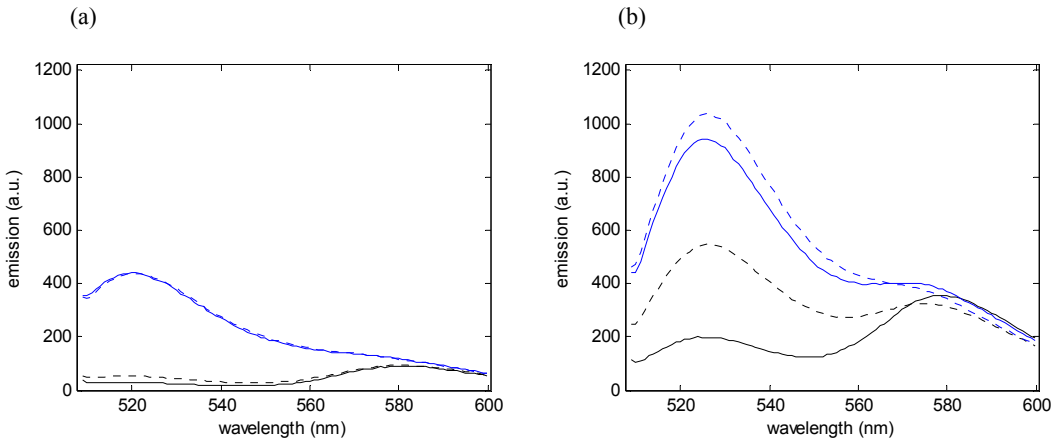

Figure 7.14. Emission of O_2O_4 (black) and O_2O_4 + $5O_3$ (blue) excited at 496 nm in a) absence and b) presence 50% PEG, with 200 mM Na^+. Solid lines indicate 24ºC and dotted lines 37ºC.

7.4 Strand exchange in polymer media

Strand exchange at 37ºC in 50% PEG is significantly faster than in PBS, attaining a yield of 100% in 30 minutes (see Figure 7.15a). Catalytic activity is present for all investigated PEG concentrations, and increases rapidly with PEG concentration. With 52.4% PEG present, the reaction is complete in 2 minutes (traces cannot be shown to scale), which implies an over 400-fold increase in the observed rate constant. Kinetic parameters for strand exchange in PEG are summarized in Table 6.

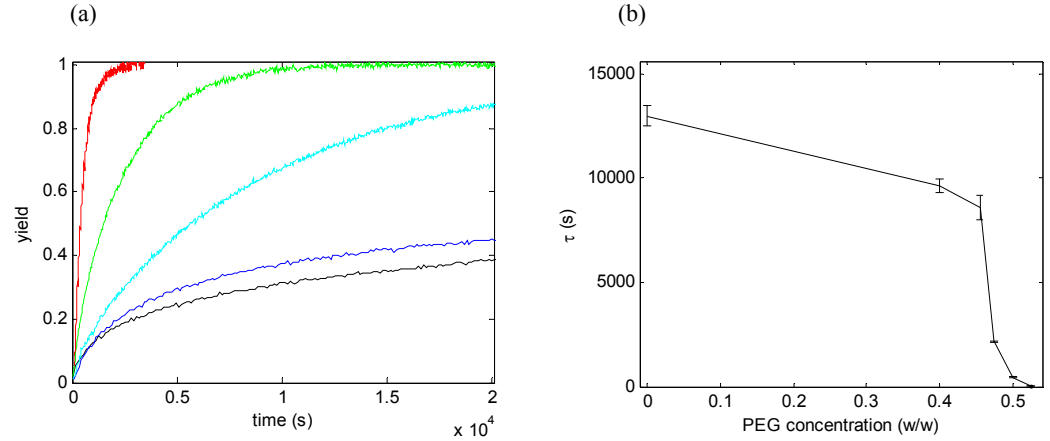

Figure 7.15. Strand exchange in PEG solution at 37ºC. a) Kinetic traces in 0.0% (black), 40.0% (blue), 45.5% (cyan), 47.4% PEG (green), and 50.0% (red) PEG. b) Inverse observed rate constants using the single exponential model (8). Error bars indicate ± standard deviation between three replicates.

At 200 mM Na^+, overall rates of strand exchange are slightly lower for all PEG concentrations except for 40% PEG which is slightly higher (see Figure 7.16). Comparing Figure 7.16a and Figure 7.15a, the initial rate of the reaction is higher at elevated salt concentration, which is to be discussed below in Chapter 8.3.

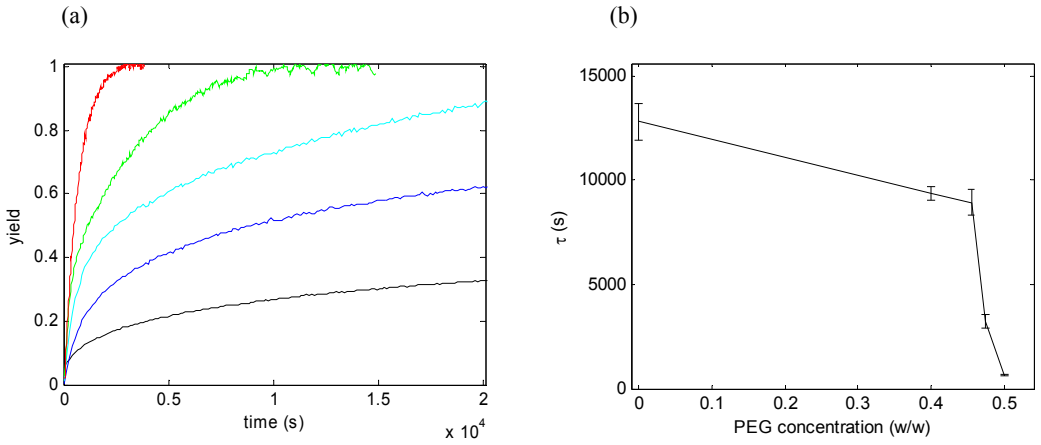

Figure 7.16. Strand exchange in PEG solution at 37ºC with 200 mM Na^+. a) Kinetic traces in 0.0% (black), 40.0% (blue), 45.5% (cyan), 47.4% PEG (green), and 50.0% (red) PEG. b) Inverse observed rate constants using the single exponential model (8). Error bars indicate ± standard deviation between three replicates.

Strand exchange is slower at 24ºC compared to at 37ºC (see Figure 7.17), although more concentrated PEG solutions still give higher yields and faster rates. Unlike at 37°C, none of the kinetic curves obtained at 24°C completes within $2 \cdot 10^4$ seconds and all of them enter a linear phase after $1 \cdot 10^4$ seconds with similar slopes.

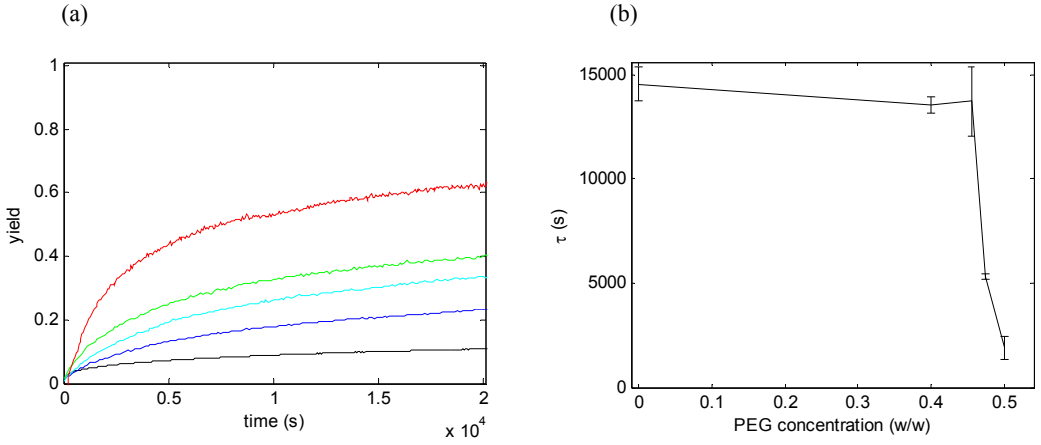

Figure 7.17. Strand exchange in PEG solution at 24ºC. a) Kinetic traces in 0.0% (black), 40.0% (blue), 45.5% (cyan), 47.4% PEG (green), and 50.0% (red) PEG. b) Inverse observed rate constants using the single exponential model (8). Error bars indicate ± standard deviation between three replicates.

The kinetics of strand exchange using mismatched dsDNA O_2m_x is considerably faster than for fully matched O_2O_4 (see Figure 7.18 and Figure 7.19a) even if it was previously found that a mismatched duplex does not have a significantly lower T_m than a matched duplex[53]. For the duplex O_2m_{10}, which is mismatched in the middle of the sequence, the rate appears to be somewhat lower than for the two other duplexes which have a mismatch at the end.

Using fully matched dsDNA and ssDNA at the proportion 1:5 causes 5/6 of the original duplexes to disappear. Mismatched duplexes dissociate completely, and therefore, should have an equilibrium emission 1.2 times the emission of matched duplexes. As shown in Figure 7.19b, the real ratio is approximately 1.35. This is similar to a value previously published[53], when the discrepancy was explained with attractive ionic interactions between FAM and TAMRA in the matched duplex which increases its stability. There is no explanation for the low yields using PEG, except for possible errors in the $O_2m_x + 5O_3$ measurements. Though the yields may be somewhat inexact, rate calculations are not affected and the discussion to follow is still valid.

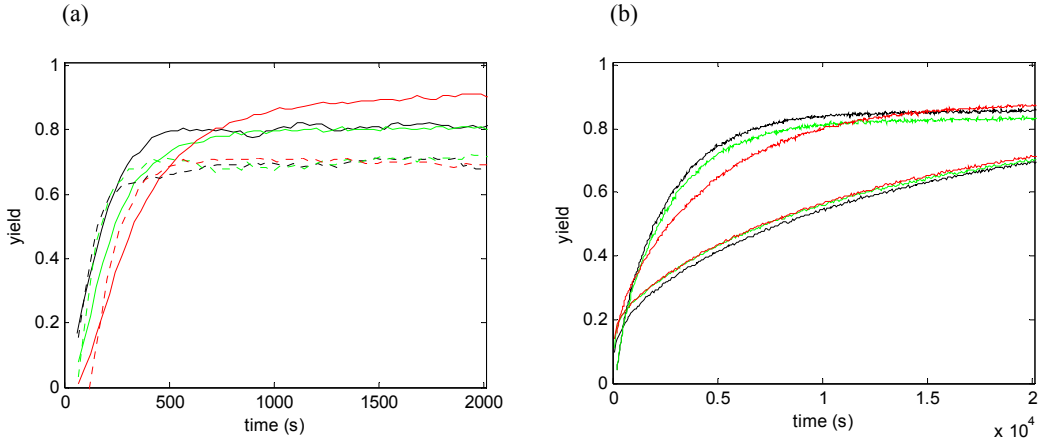

Figure 7.18. Single observations of strand exchange with mismatched DNA. a) Kinetic traces of O_2m_4 (black), O_2m_5 (green), and O_2m_{10} (red) in 47.4% (solid) and 50.0% (dotted) PEG. b) Kinetic traces in 40.0% (lower) and 45.5% (upper) PEG.

A discovered but yet unexplained peculiarity of PEG solutions is their extremely long equilibration times of several days. In Figure 7.20a, the emission spectra of FAM in newly made PEG solution differs considerably from those in equilibrated PEG. Furthermore, newly made PEG does not significantly accelerate DNA strand exchange (see Figure 7.20b).

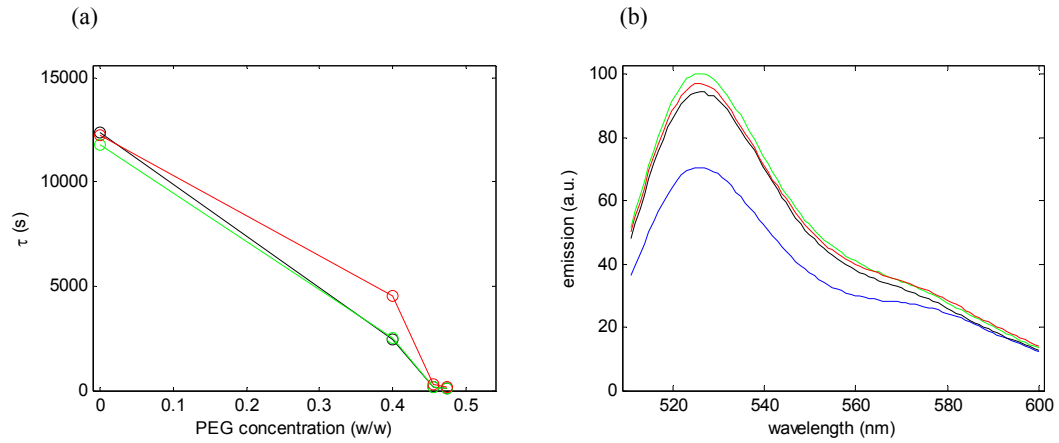

Figure 7.19. a) Inverse observed rate constants using the single exponential model (8), for O_2m_4 (black), O_2m_5 (green), and O_2m_{10} (red). b) Emission spectra of O_2O_4 + $5O_3$ (blue), O_2m_4 + $5O_3$ (black), O_2m_5 + $5O_3$ (green), and O_2m_{10} + $5O_3$ (red) in PBS when excited at 496 nm.

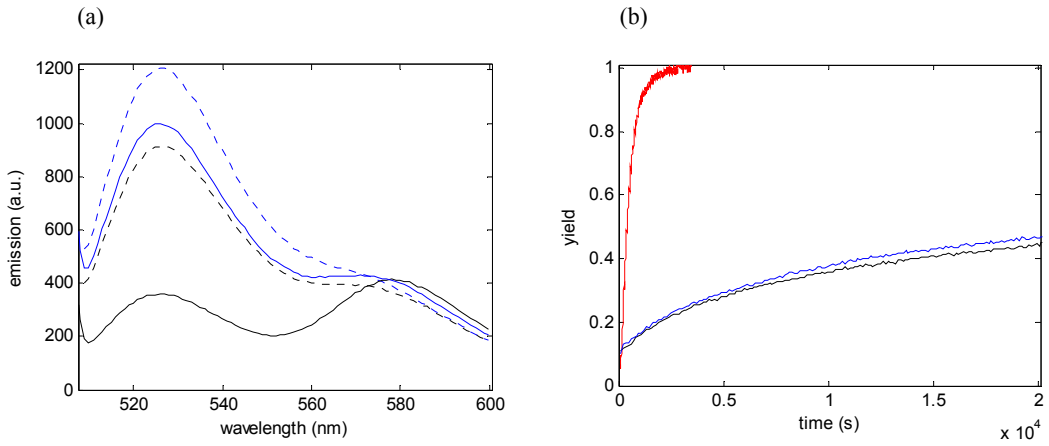

Figure 7.20. a) Emission spectra at 37ºC of O_2O_4 (black) and O_2O_4 + $5O_3$ (blue) in newly made (solid) and equilibrated (dotted) 50.0% PEG solution. b) Kinetic traces of DNA strand exchange with newly made (black), 6 hours old (blue), and equilibrated (red) 50.0% PEG solutions.

PEG was replaced with monomeric DME to investigate the importance of a hydrophobic environment without crowding. The environmental effect on DNA from 25% DME in PBS roughly corresponds to the effect from 50% PEG in PBS, since the FAM and TAMRA emission spectra in O_2O_4 appear equivalent in both solutions. Strand exchange kinetics is very similar in these two mixtures (see Figure 7.21). Although being similar in chemical composition to PEG, DME does not cause a shift of the FAM peak.

Table 6. Fitted parameters for strand exchange using PEG.

experiment	% PEG	fitted parameters		
		y_0 [a]	τ	±
50mM Na^+ 37°C 3 replicates	**0.0**	0,481	12979	468
	40.0	0,500	9625	298
	45.5	0,990	8608	581
	47.4	0,994	2158	17
	50	0,999	438	40
	52.4	1,027	43	20
200mM Na^+ 37°C 3 replicates	**0.0**	0,392	12800	875
	40.4	0,685	9377	329
	45.5	0,929	8922	631
	47.4	1,020	3235	314
	50	1,006	643	19
50µM Na^+ 24°C 3 replicates	**0.0**	0,224	14539	818
	40.0	0,291	13537	408
	45.5	0,401	13734	1667
	47.4[b]	0,385	5312	113
	47.4	0,459	9516	210
	50[b]	0,394	1910	551
	50	0,608	6404	564
50mM Na^+ 37°C mismatched O_2m_4 single experiment	**0.0**	0,826	12354	
	40.4	0,853	2421	
	45.5	0,810	145	
	47.4	0,692	100	
50mM Na^+ 37°C mismatched O_2m_5 single experiment	**0.0**	0,817	11812	
	40.4	0,828	2495	
	45.5	0,803	191	
	47.4	0,700	87	
50mM Na^+ 37°C mismatched O_2m_{10} single experiment	**0.0**	0,837	12219	
	40.4	0,879	4540	
	45.5	0,906	308	
	47.4	0,707	147	

[a] Kinetic traces of matched DNA with y_0 differing from 1 did not fit well using model (8).
[b] Instead of $4 \cdot 10^4$ s, the time frame of these fits were $1.5 \cdot 10^4$ s and $2.5 \cdot 10^3$ s, equivalent to the runs with 45.5% and 47.4% PEG.

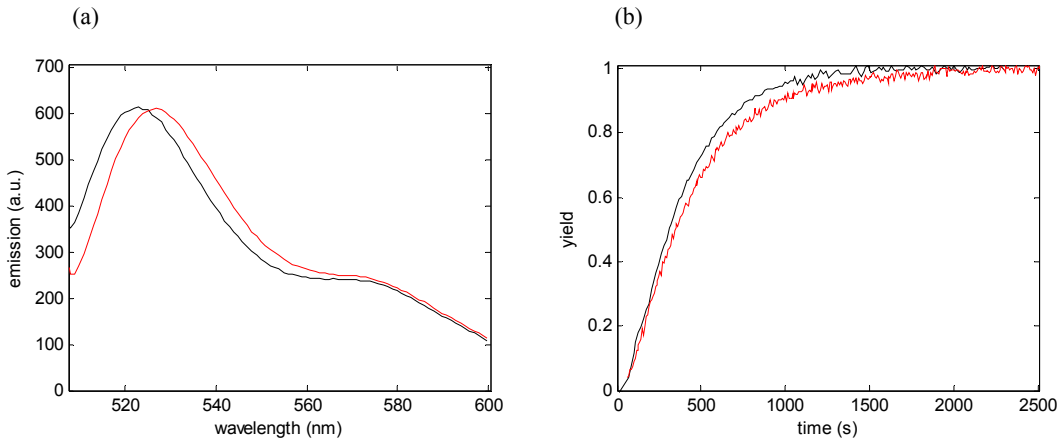

Figure 7.21. a) Emission spectra of O_2O_4 at 37ºC in 25 % DME by volume (black) and 50.0 % PEG (red) when excited at 496 nm. b) Kinetic traces of strand exchange in DME (black) and PEG (red).

It is not possible to match the emission spectra in 40% PEG using DME, but a 5% DME solution gives approximately the same FAM fluorescence intensity and also similar kinetics as shown in Figure 7.22.

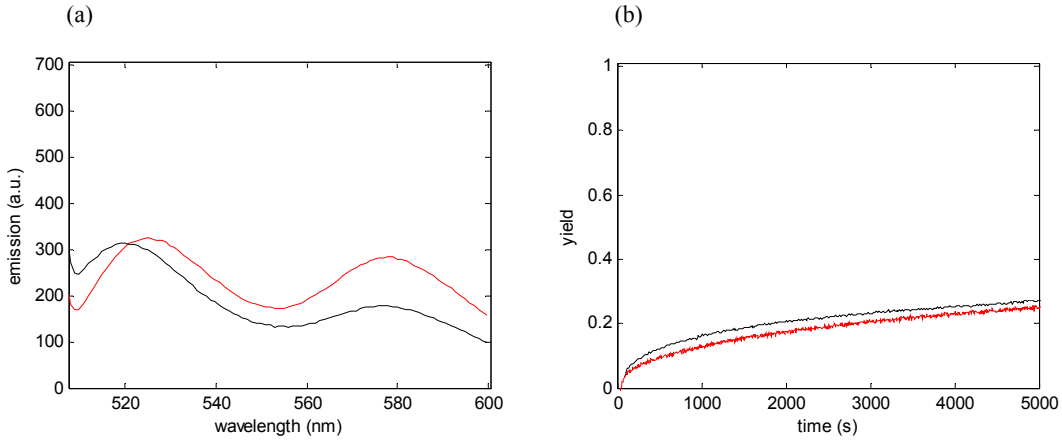

Figure 7.22. a) Emission spectra of O_2O_4 at 37ºC in 5.0% DME by volume (black) and 40.0% PEG (red) when excited at 496 nm. b) Kinetic traces of strand exchange in DME (black) and PEG (red).

Dextran was used as an alternative crowding agent to PEG. It does not shift the FAM emission peak and only slightly alters the emission spectrum of O_2O_4 (see Figure 7.23a). Strand exchange in 20% dextran is not significantly faster than in PBS (see Figure 7.23b), but the catalytic activity of PEG is also low at concentrations below 40%.

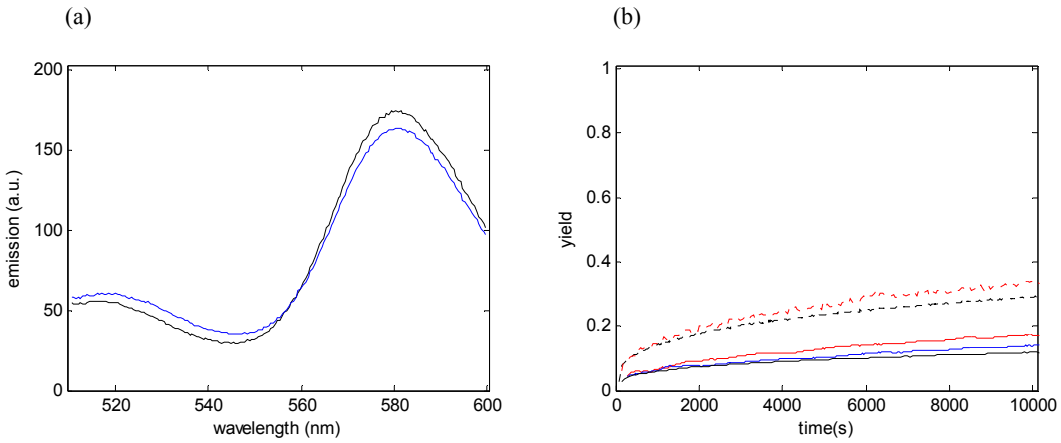

Figure 7.23. a) Emission spectra of O_2O_4 at 24ºC in 20% dextran (black) and PBS (blue) when excited at 496 nm. b) Kinetic traces of strand exchange in PBS (black), 10% dextran (blue), and 20% dextran (red) at 24ºC (solid) and 37ºC (dotted).

7.5 Curve fitting

Many of the slower kinetic traces entered a linear phase after approximately 10^4 seconds, which was poorly represented using the exponential model (8). Therefore, the improved model

$$y = y_0 - Ae^{-\frac{x}{\tau}} + Bx, \tag{9}$$

which includes a linear term, was attempted for the traces in Figure 7.17a. The time frame was $2 \cdot 10^4$ seconds. Results are presented in Table 7, Figure 7.24, and Figure 7.25. Though the r^2 values are high for model (8), it is easily seen that the curvature is poorly reproduced, resulting in y_0 values differing greatly from unity. On the other hand, model (9) fits well to experimental data, and there are no systematic variations of the residual.

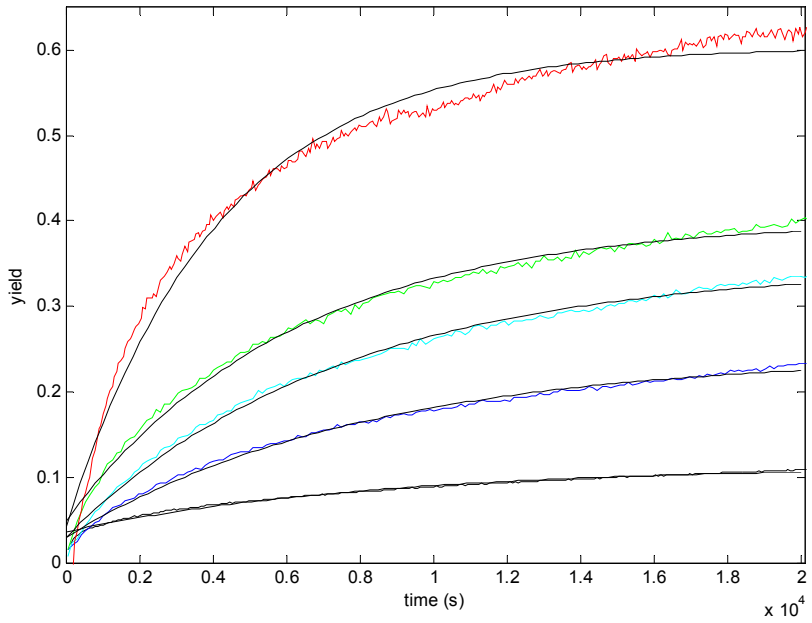

Figure 7.24. Fits (black) of kinetic traces from Figure 7.17a using model (8).

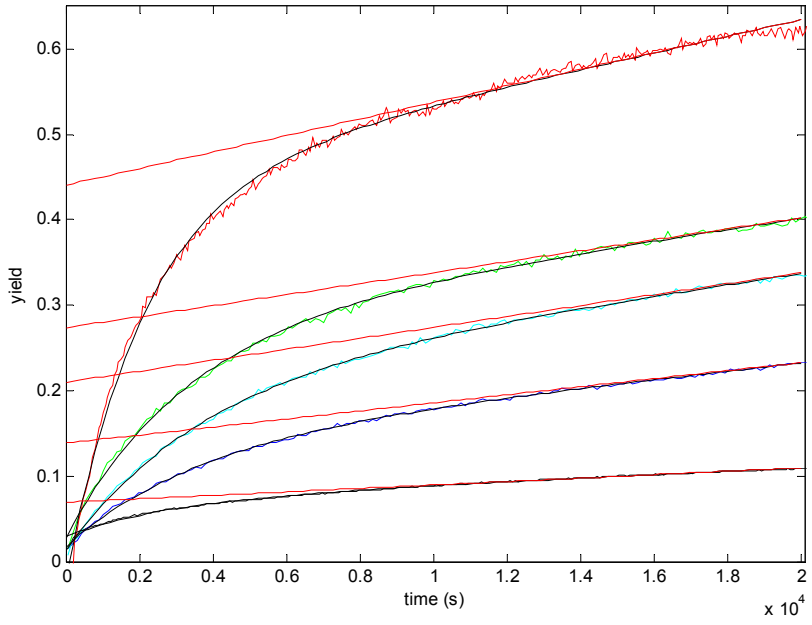

Figure 7.25. Fits (black) of kinetic traces from Figure 7.17a using the improved model (9). Linear component is plotted in red. The fit is less perfect for 50.0% PEG.

Table 7. Fitted parameters using model (8) and model (9).

model	% PEG	fitted parameter				
		y_0	A	τ	B	r^2
(8)	**0.0**	0.113	0.077	8281		0.991
	40.0	0.242	0.213	7970		0.995
	45.5	0.347	0.318	7330		0.995
	47.4	0.401	0.352	6121		0.994
	50.0	0.604	0.562	4144		0.983
(9)	**0.0**	0.069	0.041	2738	$2.017 \cdot 10^{-6}$	0.998
	40.0	0.139	0.121	3557	$4.714 \cdot 10^{-6}$	0.999
	45.5	0.210	0.197	3655	$6.390 \cdot 10^{-6}$	0.999
	47.4	0.274	0.246	3298	$6.428 \cdot 10^{-6}$	0.999
	50.0	0.441	0.464	2141	$9.685 \cdot 10^{-6}$	0.997

8 Discussion

Catalysis promoted by cationic charges and nonionic catalysis are the two main approaches to DNA strand exchange catalysis studied in this thesis, and will be discussed below in that order.

8.1 Cationic catalysis

The differences in T_m between Figure 7.4a and Figure 7.4b reflects the inability of peptides RL and KL to bind to DNA, despite carrying an equal number of formal charges compared to R7 (counting the protonated N-terminal). This illustrates the amino acid sequence dependence of polypeptide-DNA interactions. It could be argued either that the interspersed tryptophan residues of RL and KL are large enough to create a sterical repulsion effect, or that charge concentration along the polypeptide has a minimum threshold for efficient strand exchange. In any case, these results together with the marked differences between arginine and lysine found in earlier reports[55] clearly show that electrostatic binding of peptides to DNA is subject to influences from unexpected factors, and cannot be predicted solely on the number of formal charges.

Melting curves of DNA incubated with the polyarginine R7, which show a different behavior during heating and subsequent cooling, indicate the existence of two different ways of R7-DNA binding at room temperature. It can be suspected that the initial high T_m mode contains complexes of individual peptides bound to both strands of the duplex, but after melting, during which the helix unwinds and the two strands separate, each peptide is bound to only one strand. Therefore some of the additional DNA duplex stability is lost. Though not investigated, this second mode of binding, which has lower absorbance (compare solid and dotted lines in Figure 7.4b) and thus is more compact, may exhibit different strand exchange kinetics.

Since R7 promotes strand exchange while increasing T_m of the double helix, it lowers both the reactant and product free energies. Its catalytic effect must therefore originate in the ability to attract and compact several DNA strands at once, pulling ssDNA and dsDNA together by force, thereby lowering the electrostatic repulsion barrier of an intermediary three stranded complex. At peptide:dsDNA charge ratios higher than 1 however, yields were discovered to decrease substantially (see Figure 7.6b), which can be explained by cooperative formation of highly compacted dsDNA-peptide and ssDNA-peptide complexes unable to participate in strand invasion. This last conjecture is supported by the quickly decreasing TAMRA fluorescence in Figure 7.5b, and the fact that yields are even lower for higher R7 concentrations with maintained stoichiometry.

While no usable results were obtained with peptides immobilized on beads, the use of negatively charged liposomes to electrostatically attract the peptides and thereby create a catalytic surface was more successful. Liposomes together with R7 had an activity which was higher than that of 35% DOTAP liposomes containing 3% DSPE-MPEG, and at low concentration also higher than the activity of 35% DOTAP liposomes (see Figure 7.7). However, the yields were worse in presence of liposomes than using the equivalent amount

of free peptides in solution, which shows that there is no additional positive contribution from a two-dimensional arrangement. It can furthermore be suspected that a comparatively large fraction of the peptides eventually dissociate from the liposomes.

In the light of the results in this thesis, one unclear point remains regarding earlier studies[12,55] using polypeptides to catalyze strand exchange. It was reported that the surfactant SDS was added to the DNA samples to prevent the polyarginines from quenching fluorescence. Such a methodology would be flawless had SDS not been known to enhance the rate of DNA intercalation.[77] It could be suspected that the role of arginine was mainly to compact and concentrate DNA, and that addition of anionic SDS, attracted to cationic arginine, actually constitutes another example of hydrophobic catalysis.

8.2 Hydrophobic catalysis

The existence of an optimal peptide:DNA charge ratio, which is evident from Figure 7.6b, suggests that each recombinase unit can only contain a few charged amino acid residues to prevent excessive *in vivo* DNA aggregation. Indeed, a relatively limited number of cationic charges are found in the RecA filament when accommodating a triple stranded DNA intermediate. However, results presented in this thesis show that cationic charges at low density or at low concentrations do not correlate with a fast reaction *in vitro* (see Table 4). It can therefore be deduced that other factors than charge must contribute to enzyme activity.

The crowded and nonpolar environment inside the RecA filament can be recreated in a model system using PEG. Several arguments based on the results obtained support that PEG genuinely catalyzes DNA strand exchange, and that the recovery of FAM emission is not simply due to O_2O_4 melting. Firstly, catalytic activity remains at a high salt concentration which stabilizes the duplex. T_m of DNA in 50% PEG with 200 mM Na^+ is actually higher than T_m of DNA in PBS with 50 mM Na^+, while strand exchange is significantly faster. This very important result demonstrates that DNA strand exchange activity can differ significantly from its thermodynamic stability. Previous reports[13,57] of this principle were not based on free B-DNA in solution. Secondly, no strand exchange was observed in presence of PEG when replacing O_3 with the fully mismatched sequence M (results not shown) as a negative control. Thirdly, CD spectra show that an overall B-DNA double helix conformation is maintained in 50% PEG at 37°C, which is consistent with earlier reports using lower PEG concentrations[73].

As seen in Appendix 1, O_2 and O_2O_3 fluorescence do increase in PEG solutions compared to in PBS, but the difference between in 40% PEG and in 50% PEG is small. The direct influence of a PEG-rich environment on the fluorophore itself does not account for the observed increase in O_2O_4 emission for higher PEG concentrations. Instead, this can be explained by dynamic end fraying of the DNA duplex, which increases the average distance between the two strands. This could be promoted by the presence of favorable hydrophobic interactions between DNA bases and nonpolar PEG chains in an environment with low water activity, similar to how the hydrophobic RecA L2 loop interacts with ssDNA. The melting curve baseline is flatter with PEG present (see Figure 7.11a), which indicates a better defined melting and slower thermal fluctuations. Therefore, it is more likely that PEG prolongs the lifetime of a single opening event, than increasing the frequency of such events. In other

words, PEG seems to grab exposed DNA bases, rather than pushing them out from the helix. Also, the incoming single strand may lose its coiled appearance in a nonpolar media and adopt an elongated state where its hydrophobic bases are more easily accessible. However, the conformation of the three stranded intermediate cannot be deduced, it could either be a three strand junction, or aided by PEG[70], a triplex with nonstandard base pairing.

The strong dependency of catalytic activity on temperature, but not directly on T_m, could be due to a combination of two effects. Firstly, the hydrophobic character of PEG increases with temperature.[78] Secondly, addition of salt shields the electrostatic repulsion between the backbones, but has little effect on the bases. Therefore, breathing and base flipping occurs equally well no matter the ionic strength, but more frequently at high than low temperature due to thermal dynamics.

The experiments with DNA strand exchange in DME (Figure 7.21 and Figure 7.22), a very short PEG analog with the same functional groups but with negligible volume of exclusion, is a strong piece of evidence in support of catalysis through hydrophobic interactions. Though not extensively studied, initial experiments seem to show a good agreement between kinetic traces obtained in DME and PEG. Since FAM fluorescence is shifted by PEG and not by DME, it cannot be proved that the DNA microenvironment is equivalent in both solutions.

Strand exchange involving mismatched DNA in PEG solution shows less difference between the mismatch positions than in earlier studies[53]. This is a sign that PEG stabilizes breathing as well as fraying ends. If it is true that the double helix is mainly stabilized through hydrophobic stacking forces, further research could show an increased occurrence of base flipping in addition to breathing, due to a decreased stacking efficiency in a nonpolar environment. Either breathing or flipping in dsDNA will create favorable sites for strand invasion performed by incoming ssDNA.

The experiments using mismatched DNA illustrate another important principle. Strand exchange *in vivo* is required to be much more selective than 1 mismatch per 20 bases. Cationic catalysis will counteract sequence specificity, since matched and mismatched DNA strands are equally well attracted by the catalyst. Hydrophobic catalysis, which promotes ssDNA strand invasion at the site of mismatch due to the permanent single stranded bubble, causes mismatched duplexes (O_2m_x) to disappear quickly in favor of matched ones (O_2O_3).

8.3 Effects from molecular crowding and diffusion

The excluded volume effect from PEG is not negligible. As demonstrated in Chapter 7.5, kinetic traces begin as exponential, but eventually enter a linear phase. This behavior can be explained using a two-step model, with a fast core reaction but a slow diffusion, presented in Figure 8.1.

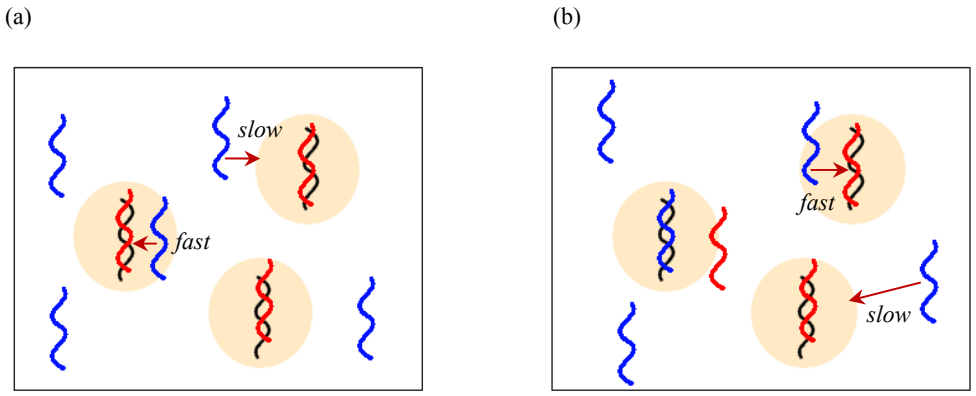

Figure 8.1. Simplified picture of diffusion limited strand exchange. The volume of immediate diffusion (spheres) is small enough to sustain the fast core reaction according to the single exponential model (1). a) The initial situation with three doubly labeled duplexes (black/red), one of which happens to have an unlabeled single strand (blue) in its volume of immediate diffusion. The kinetic trace produced is exponential. b) When the population of accessible unlabeled single strands has been depleted, continued reaction is sustained by slow diffusion of new ssDNA into the vicinity of remaining doubly labeled duplexes. The kinetic trace produced is linear, since the influx of ssDNA is constant if the yield is low and the concentrations of unreacted duplexes and ssDNA are pseudoconstant.

Comparing the kinetic traces in Figure 7.15a, Figure 7.16a, and Figure 7.17a, it becomes evident that the importance of diffusion decreases with more PEG present. Firstly, the effective concentration of unlabeled ssDNA is larger according to Figure 4.1a, so more doubly labeled dsDNA molecules begin with an ssDNA in its volume of immediate diffusion. Secondly, the volume displaced by PEG shortens the diffusion path, so the influx of ssDNA becomes sufficient to sustain continued exponential kinetics.

Furthermore, diffusion seems more limiting to the overall strand exchange reaction at high salt concentration and at low temperature. Initial kinetics is evidently faster in PEG with 200 mM instead of 50 mM Na^+ present. Meanwhile, salt concentration theoretically does not affect diffusion rate. Diffusion at 37°C is sufficient to sustain the core reaction with 50 mM Na^+, but not the faster core reaction at 200 mM Na^+. Therefore, many more of the traces in Figure 7.16a than in Figure 7.15a show linear behavior. The somewhat counterintuitive observation that the core reaction is accelerated by increasing the ionic strength suggests that electrostatic repulsion between the double helix and the invading single strand is relatively more important than the repulsion between the two strands in the helix.

When temperature is lowered from 37°C to 24°C, diffusion seems to slow down even more than the core reaction, and the linear behavior of kinetic traces is very obvious in Figure 7.17a or Figure 7.25. The fact that DNA strand exchange at lower temperatures is strongly limited by diffusion, unlike reactions involving smaller substrates, implies that the strand exchange activation energy obtained through Arrhenius plots[52] can be very misleading.

Dextran could in theory act as a pure crowding agent without hydrophobic interactions due to its hydrophilic character, but no clear catalytic activity was found. Since dextran solutions quickly increase in viscosity and stickiness with concentration, it is not feasible to use more than 20% dextran with current experimental setup.

8.4 Mathematical considerations

As shown in chapter 5.1, it is possible in theory to inflate the observed rate constant through manipulating the initial concentrations. It should be noted that this affects both right hand side factors of the expression

$$rate\ of\ disappearance = rate\ constant \cdot substrate\ concentration.$$

Without knowing the local substrate concentration, it is impossible to calculate the true rate constant from the observed rate constant. It is therefore debatable whether attempts at strand exchange catalysis solely relying on increasing the local DNA concentration, using electrostatic attractions or crowding by polymers without hydrophobic effect, constitutes real catalysis more than simply starting in a smaller volume.

The results obtained with R7 demonstrate this problem practically, since several different rates as well as yields are obtained for the same catalyst when changing DNA concentrations. There is a tradeoff between rate and yield for strand exchange in very high peptide concentrations, which shows that it is not sufficient to compare rates only. Comparing yields is also difficult, since a catalyzed system quickly reaches 100% yield compared to an uncatalyzed system. The ratio between catalyzed and uncatalyzed yields is therefore highly time dependent.

In this thesis, curve fitting has been limited to $4 \cdot 10^4$ seconds for all traces which do not reach 100% due to experimental time constraints. This cutoff severely distorts results for slow reactions, since the fitted τ parameter in model (1) increases with the time frame and tends towards infinity for the linear phase (see Figure 8.2). Importantly, the noncatalyzed strand exchange reaction fits very badly to the single exponential model. Over a short time frame, the rate constant is fairly large. Therefore, it is not entirely valid to report the catalyzed rate constant in magnitudes of uncatalyzed; nevertheless this has been done by previous authors[52,55].

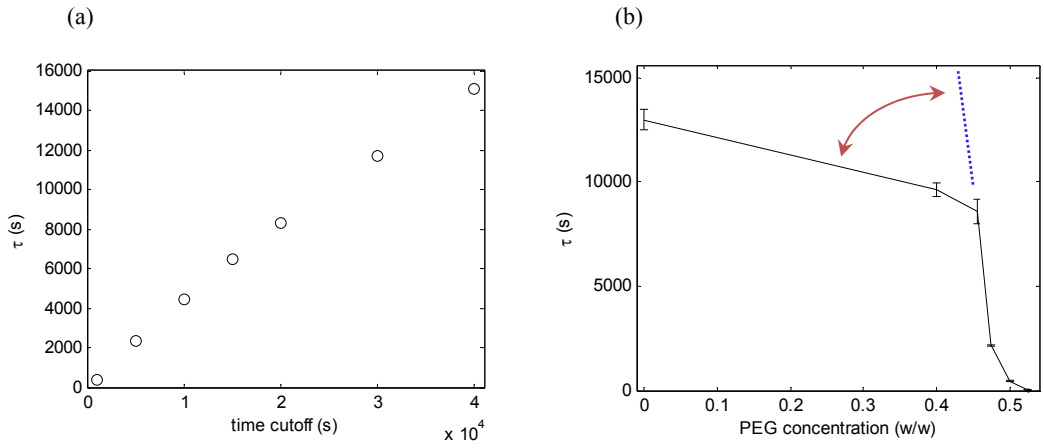

Figure 8.2. The importance of time frame cutoff on the fitted τ parameter. a) The fitted τ parameter for the uncatalyzed reaction at 24ºC for different time frames. b) Similar to Figure 7.15b, but including a hypothetical graph without time frame cutoff for the lower PEG concentrations (blue).

Lastly, a pitfall which applies to all studies of strand exchange is the importance of a correct FI_∞ value. As an example, in this thesis, the fully mismatched strand M was used as a negative control, since its sequence prohibits strand invasion. The value of FI_∞ used was that of $O_2O_4 + 5O_3$. An actual fluorescence reading of $O_2O_4 + 5M$ would have been very close, if not equal, to FI_0. A minimal number of strand exchange events would therefore constitute 100 % yield, plus an extremely fast rate, using the flawed approach. As a parallel, it is certainly possible to construct a false catalyst which irreversibly binds to a large proportion of the available unreacted dsDNA, leaving a small population quickly depleted. Interpreting these results carelessly would yield very misleading results.

9 Conclusions

The results obtained suggest that DNA strand exchange is initiated by spontaneous appearance of local single strands in the double helix, and proceeds via a three stranded intermediate complex. Fraying ends and single stranded bubbles can be stabilized by a nonpolar environment through favorable hydrophobic interactions, thereby decreasing the activation energy barrier.

Fundamentally different from the previously studied ionic catalysts, PEG combines hydrophobic interactions with molecular crowding. Catalytic activity is not lost with increased ionic strength. The stability contribution from base stacking and the interactivity between DNA and a nonpolar environment appears more important to DNA activity than previously realized.

While the core strand exchange reaction proceeds according to monoexponential kinetics, it is limited by long range diffusion. Molecular crowding decreases the importance of diffusion and feeds new ssDNA to unreacted dsDNA through a push mechanism due to volume exclusion.

Charge based catalysis works by stabilizing the three stranded intermediate and increasing the local DNA concentration through electrostatic traction to sustain the reaction. Cationic peptides provide a balance between fast rate or high yield, and their catalytic activity is equally dependent on peptide sequence as charge.

DNA in PEG solutions is subjected to an environment similar to that inside the recombinase-DNA complex filament, with molecular crowding and hydrophobic forces more dominating than charge-charge interactions. While concentrated positive charges can be important to filament assembly, the results in this thesis indicate that the strand exchange reaction is mainly driven by nonionic forces.

10 Future work

It was not possible to obtain thermodynamic data for helix stabilization from the melting curves, since flat baselines could not be obtained (see Figure 7.4). Although strand exchange would become impractically slow, the use of longer DNA in melting curve experiments would yield flat baselines, so a direct comparison of DNA stability in PEG solutions and in PBS becomes possible.

The FAM-TAMRA energy transfer pair is not ideal, since FAM quantum yield in single and double strands is different, and TAMRA is excited at the FAM absorption maximum. Furthermore, FAM and TAMRA interact electrostatically which may distort DNA strand exchange activity. The possibility of using other fluorophores should be investigated, as well as multiple fluorophores per strand to monitor strand dynamics.

By labeling ssDNA and the strand in dsDNA with identical sequence, the existence of a triple stranded intermediate, junction or triplex, could be investigated. Such an intermediate would be very different using helix stabilizing and helix destabilizing catalysts. It may be possible to deduce the real rate constant of strand exchange by knowing the number of intermediates present.

It is possible to anchor R7 to a membrane using hydrophobic anchor groups, which will allow the use of much higher charge density without creating large peptide-DNA complexes. Overall, strand exchange in the high charge density region is an interesting engineering concept even if there is no apparent biological counterpart.

It is not known why 26% DME, which due to its small molecular size creates a negligible excluded volume, can sustain strand exchange. Experiments in the interval 5% to 26% are needed. Furthermore, it is unknown if other small nonpolar but water-soluble molecules, or hydrogen bond disrupting molecules like urea and formamide, can catalyze strand exchange.

Lastly, the ratio between ssDNA reacting directly and through diffusion control, which is simply the intercepts of the linear components in Figure 7.25, may be used to investigate the microenvironment of each DNA strand. It would theoretically be possible to calculate the real volume available by correlating yields to the volume occupied by PEG. Taking advantage of the fact that the strand exchange reaction, unlike many other reactions, is limited by diffusion, it could be possible in the future to use DNA strands to probe the size of small enclosed volumes in micelles, zeolites, and similar.

11 Acknowledgements

First my gratitude goes to my examiner Bengt Nordén, for all our discussions together and for your patience and enthusiasm, for the great opportunity to work at the department and with members of your group. Thank you for your confidence in me to complete this fascinating project and for being a source of inspiration and a steady locomotive force from the first day to the last; this project would not be possible without your excellent leadership.

Likewise my gratitude goes to my supervisor Karolin Frykholm and my co-supervisors Fredrik Westerlund and Anna Reymer; for all the help and guidance during the project, theoretically as well as practically. Thank you Karolin, for literally sharing your pipettes for a whole year, and too much of your lab space, for answering my questions, big, small, and silly, for your magic ability to solve problems which look impossible, and for your knowledge and encouragement when things look hopeless as well as successful. Thank you Fredrik, for a never ending torrent of ideas advancing the project, for lots of help in experimental planning, for both of us thinking critically, and for reading and improving and yet again proofreading my thesis drafts. Thank you Anna for introducing me to proteins, DNA, and everything, for teaching me the value of knowledge, molecular modeling, and the wonderful world *in silico*, and for valuable advice when writing my thesis.

Thank you all, examiner and supervisors, for allowing me to explore Science at its best; I appreciate that you trusted me to work independently yet never being far away, to let me develop my skills at scientific research; all of what I have learned from you cannot be expressed in words.

For valuable discussions and scientific advice, special thanks go to Björn Åkerman and Erik Lundberg about DNA, to Per Lincoln about kinetics, to Staffan Wall about polymers, to Tommy Gustafsson about mathematics, and to Johan Bergenholtz about PEG. To Joakim Andréasson, Joakim Kärnbratt, and Marcus Wilhelmsson about fluorescence. To Morten Grøtli, Nina Kann, and Jerker Mårtensson about organic chemistry. Special thanks go to Aldo Jesorka for invaluable help with HPLC and to Kristina Fant with the fluorometer, and to Göran Svensson and Nikola Markovic for your problem solving capabilities. To Helene Åmand for fluorescein, and Martin Hammarson and Jonas Hannestad for DNA. To Nils Carlsson for solving the mystery of the sixth cell, and to whom I owe a lot.

Thank you, Calin Plesa and Sofie Ståhl, for reading my lengthy draft and agreeing to be my opponents, and all the other numerous diploma workers for being nice roommates in a tight space. Thank you for our journey at Chalmers together.

Finally, I would like to thank every single person of the Division of Physical Chemistry, you have all helped me, for a wonderful, friendly, and welcoming atmosphere, for good company while performing lengthy experiments, for tips and tricks in the laboratory, and for maintaining the highest standards of excellence.

References

(1) Crick, F. *Nature* 1970, *227*, 561.

(2) Kowalczykowski, S. C.; Dixon, D. A.; Eggleston, A. K.; Lauder, S. D.; Rehrauer, W. M. *Microbiol Rev* 1994, *58*, 401.

(3) Baumann, P.; West, S. C. *Trends Biochem Sci* 1998, *23*, 247.

(4) Kowalczykowski, S. C.; Eggleston, A. K. *Annu Rev Biochem* 1994, *63*, 991.

(5) Chen, Z.; Yang, H.; Pavletich, N. P. *Nature* 2008, *453*, 489.

(6) Reymer, A.; Frykholm, K.; Morimatsu, K.; Takahashi, M.; Norden, B. *Proc Natl Acad Sci U S A* 2009, *106*, 13248.

(7) Nomme, J.; Takizawa, Y.; Martinez, S. F.; Renodon-Corniere, A.; Fleury, F.; Weigel, P.; Yamamoto, K.; Kurumizaka, H.; Takahashi, M. *Genes Cells* 2008, *13*, 471.

(8) Lavery, P. E.; Kowalczykowski, S. C. *J Biol Chem* 1990, *265*, 4004.

(9) Stohl, E. A.; Brockman, J. P.; Burkle, K. L.; Morimatsu, K.; Kowalczykowski, S. C.; Seifert, H. S. *J Biol Chem* 2003, *278*, 2278.

(10) McGrew, D. A.; Knight, K. L. *Crit Rev Biochem Mol Biol* 2003, *38*, 385.

(11) Frykholm, K.; Bombelli, F. B.; Nordén, B.; Westerlund, F. *Soft Matter* 2008, *4*, 2500.

(12) Tajima, K.; Kim, W. J.; Akaike, T.; Maruyama, A. *Nucleic Acids Res Suppl* 2002, 265.

(13) Kim, W. J.; Ishihara, T.; Akaike, T.; Maruyama, A. *Chemistry* 2001, *7*, 176.

(14) Bloomfield, V. A.; Crothers, D. M.; Tinoco, I. *Nucleic acids : structures, properties, and functions*; University Science Books: Sausalito, Calif., 2000.

(15) Maniatis, T.; Venable, J. H., Jr.; Lerman, L. S. *J Mol Biol* 1974, *84*, 37.

(16) Watson, J. D.; Crick, F. H. *Nature* 1953, *171*, 737.

(17) Fonseca Guerra, C.; Bickelhaupt, F. M.; Snijders, J. G.; Baerends, E. J. *J Am Chem Soc* 2000, *122*, 4117.

(18) Protozanova, E.; Yakovchuk, P.; Frank-Kamenetskii, M. D. *J Mol Biol* 2004, *342*, 775.

(19) Yakovchuk, P.; Protozanova, E.; Frank-Kamenetskii, M. D. *Nucleic Acids Res* 2006, *34*, 564.

(20) Luo, R.; Gilson, H. S.; Potter, M. J.; Gilson, M. K. *Biophys J* 2001, *80*, 140.

(21) Sen, A.; Nielsen, P. E. *Biophys Chem* 2009, *141*, 29.

(22) Kool, E. T. *Annu Rev Biophys Biomol Struct* 2001, *30*, 1.

(23) Friedman, R. A.; Honig, B. *Biophys J* 1995, *69*, 1528.

(24) Sen, A.; Nielsen, P. E. *Nucleic Acids Res* 2007, *35*, 3367.

(25) Feuerstein, B. G.; Pattabiraman, N.; Marton, L. J. *Proc Natl Acad Sci U S A* 1986, *83*, 5948.

(26) Anastassopoulou, J.; Theophanides, T. *Crit Rev Oncol Hematol* 2002, *42*, 79.

(27) Forster, W.; Bauer, E.; Schutz, H.; Berg, H.; Akimenko, M.; Minchenkova, L. E.; Evdokimov Yu, M.; Varshavsky Ia, M. *Biopolymers* 1979, *18*, 625.

(28) Breslauer, K. J.; Frank, R.; Blocker, H.; Marky, L. A. *Proc Natl Acad Sci U S A* 1986, *83*, 3746.

(29) Sugimoto, N.; Nakano, S.; Yoneyama, M.; Honda, K. *Nucleic Acids Res* 1996, *24*, 4501.

(30) SantaLucia, J., Jr.; Allawi, H. T.; Seneviratne, P. A. *Biochemistry* 1996, *35*, 3555.

(31) Dervan, P. B. *Science* 1986, *232*, 464.

(32) Vazquez, M. E.; Caamano, A. M.; Mascarenas, J. L. *Chem Soc Rev* 2003, *32*, 338.

(33) Alberts, B.; Wilson, J. H.; Hunt, T. *Molecular biology of the cell*; 5th ed.; Garland Science: New York, 2008.

(34) Gueron, M.; Kochoyan, M.; Leroy, J. L. *Nature* 1987, *328*, 89.

(35) Frank-Kamenetskii, M. *Nature* 1987, *328*, 17.

(36) Bicout, D. J.; Kats, E. *Phys Rev E Stat Nonlin Soft Matter Phys* 2004, *70*, 010902.

(37) Altan-Bonnet, G.; Libchaber, A.; Krichevsky, O. *Phys Rev Lett* 2003, *90*, 138101.

(38) Lee, O. C.; Jeon, J. H.; Sung, W. *Phys Rev E Stat Nonlin Soft Matter Phys* 2010, *81*, 021906.

(39) Suck, D. *Curr Biol* 1994, *4*, 252.

(40) Roberts, R. J.; Cheng, X. *Annu Rev Biochem* 1998, *67*, 181.

(41) Huang, N.; MacKerell, A. D., Jr. *Philos Transact A Math Phys Eng Sci* 2004, *362*, 1439.

(42) Kafri, Y.; Mukamel, D.; Peliti, L. *Phys Rev Lett* 2000, *85*, 4988.

(43) Varnai, P.; Lavery, R. *J Am Chem Soc* 2002, *124*, 7272.

(44) Allan, B. W.; Beechem, J. M.; Lindstrom, W. M.; Reich, N. O. *J Biol Chem* 1998, *273*, 2368.

(45) Fuxreiter, M.; Luo, N.; Jedlovszky, P.; Simon, I.; Osman, R. *J Mol Biol* 2002, *323*, 823.

(46) Allan, B. W.; Reich, N. O. *Biochemistry* 1996, *35*, 14757.

(47) Selmane, T.; Wittung-Stafshede, P.; Maraboeuf, F.; Voloshin, O. N.; Norden, B.; Camerini-Otero, D. R.; Takahashi, M. *FEBS Lett* 1999, *446*, 30.

(48) Singleton, S. F.; Xiao, J. *Biopolymers* 2001, *61*, 145.

(49) Lavery, P. E.; Kowalczykowski, S. C. *J Biol Chem* 1992, *267*, 9307.

(50) Cox, M. M.; Lehman, I. R. *J Biol Chem* 1982, *257*, 8523.

(51) Broker, T. R.; Lehman, I. R. *J Mol Biol* 1971, *60*, 131.

(52) Kim, W. J.; Akaike, T.; Maruyama, A. *J Am Chem Soc* 2002, *124*, 12676.

(53) Frykholm, K.; Norden, B.; Westerlund, F. *Langmuir* 2009, *25*, 1606.

(54) Reynaldo, L. P.; Vologodskii, A. V.; Neri, B. P.; Lyamichev, V. I. *J Mol Biol* 2000, *297*, 511.

(55) Tajima, K.; Kim, W. J.; Sato, Y.; Akaike, T.; Maruyama, A. *Chemistry Letters* 2003, *32*, 470.

(56) Torigoe, H.; Ferdous, A.; Watanabe, H.; Akaike, T.; Maruyama, A. *J Biol Chem* 1999, *274*, 6161.

(57) Choi, S. W.; Kano, A.; Maruyama, A. *Nucleic Acids Res* 2008, *36*, 342.

(58) Minton, A. P. *J Cell Sci* 2006, *119*, 2863.

(59) Ellis, R. J. *Trends Biochem Sci* 2001, *26*, 597.

(60) Miyoshi, D.; Sugimoto, N. *Biochimie* 2008, *90*, 1040.

(61) Minton, A. P. *Curr Opin Struct Biol* 2000, *10*, 34.

(62) Lukacs, G. L.; Haggie, P.; Seksek, O.; Lechardeur, D.; Freedman, N.; Verkman, A. S. *J Biol Chem* 2000, *275*, 1625.

(63) Han, J.; Herzfeld, J. *Biophys J* 1993, *65*, 1155.

(64) Harris, J. M.; Zalipsky, S.; American Chemical Society. Division of Polymer Chemistry.; American Chemical Society. Meeting *Poly(ethylene glycol) : chemistry and biological applications*; American Chemical Society: Washington, DC, 1997.

(65) Albertsson, P. Å. *Partition of cell particles and macromolecules; distribution and fractionation of cells, viruses, microsomes, proteins, nucleic acids, and antigen-antibody complexes in aqueous polymer two-phase systems*; J. Wiley: New York,, 1960.

(66) Kanai, R.; Edwards, G. E. *Plant Physiol* 1973, *52*, 484.

(67) Lüsse, S.; Arnold, K. *Macromolecules* 1996, *29*, 4251.

(68) Rajulu, A. V.; Sab, P. M. *Eur Polym J* 1996, *32*, 267.

(69) Graham, N. B.; Chen, C. F. *Eur Polym J* 1993, *29*, 149.

(70) Spink, H.; Chaires, J. B. *J Am Chem Soc* 1995, *117*, 12887.

(71) Ninni, L.; Camargo, M. S.; Meirelles, A. J. A. *Thermochimica Acta* 1999, *328*, 169.

(72) Karimata, H.; Nakano, S.; Ohmichi, T.; Kawakami, J.; Sugimoto, N. *Nucleic Acids Symp Ser (Oxf)* 2004, 107.

(73) Nakano, S.; Karimata, H.; Ohmichi, T.; Kawakami, J.; Sugimoto, N. *J Am Chem Soc* 2004, *126*, 14330.

(74) Cheng, S. M.; Mohr, S. C. *FEBS Lett* 1974, *49*, 37.

(75) Lakowicz, J. R. *Principles of fluorescence spectroscopy*; 2nd ed.; Kluwer Academic/Plenum: New York, 1999.

(76) Klonis, N.; Clayton, A. H.; Voss, E. W., Jr.; Sawyer, W. H. *Photochem Photobiol* 1998, *67*, 500.

(77) Westerlund, F.; Wilhelmsson, L. M.; Norden, B.; Lincoln, P. *J Am Chem Soc* 2003, *125*, 3773.

(78) Jönsson, B. *Surfactants and polymers in aqueous solution*; John Wiley & Sons: Chichester ; New York, 1998.

Appendix 1. Emission spectra for fluorescently labeled DNA strands

Solid lines indicate 24°C, while dotted lines indicate 37°C.

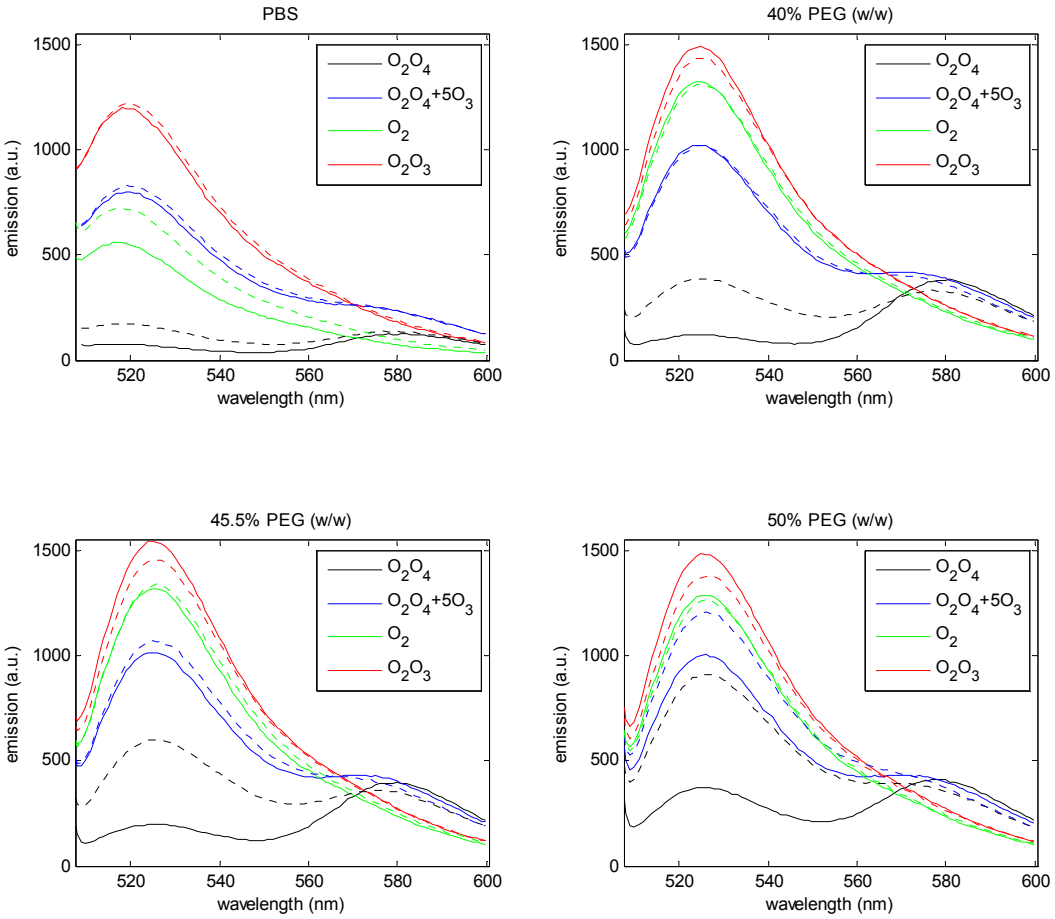

Appendix 2. Synthesis of peptide coated beads

The coating of Dynabeads Myone Carboxylic Acid with R7 was performed according to the one-step coating procedure in revision 003 of the instructions provided by Invitrogen. EDC was used as a coupling agent between the N-terminal of the peptide and the carboxylic acid groups. The compositions of buffers were according to the following list.

25 mM MES buffer (pH 6): 0.53 g 2-(N-morpholino)ethanesulfonic acid (MES) in 100 mL distilled water.

0.05 M Tris buffer (pH 7.4): 0.79 g Tris HCl in 100 mL distilled water.

EDC solution: 10 mg/mL 1-Ethyl-3-(3-dimethylaminopropyl)carbodiimide (EDC) in cold MES.

1 mg beads (100 µL) was washed two times with equal volume MES and mixed for 20 minutes in total. 600 pmol peptide was added and slowly mixed for 30 minutes. 10 µL EDC solution was added and vortexed, and the total volume was adjusted to 40 µL by adding MES. The reaction tube was incubated over night at approximately 8°C. Remaining unreacted carboxylic acid groups were blocked by washing with 100 µL Tris buffer four times.